AD-A161 338 DEVELOPMENT OF SPACECRAFT MATERIALS AND STRUCTURES FUNDAMENTALS..(U) GENERAL ELECTRIC CORPORATE RESEARCH AND DEVELOPMENT SCHENECTA.. S PROCHAZKA ET AL. AUG 85 1/1

UNCLASSIFIED SRD-85-021 AFOSR-TR-85-0974 F/G 11/2 NL

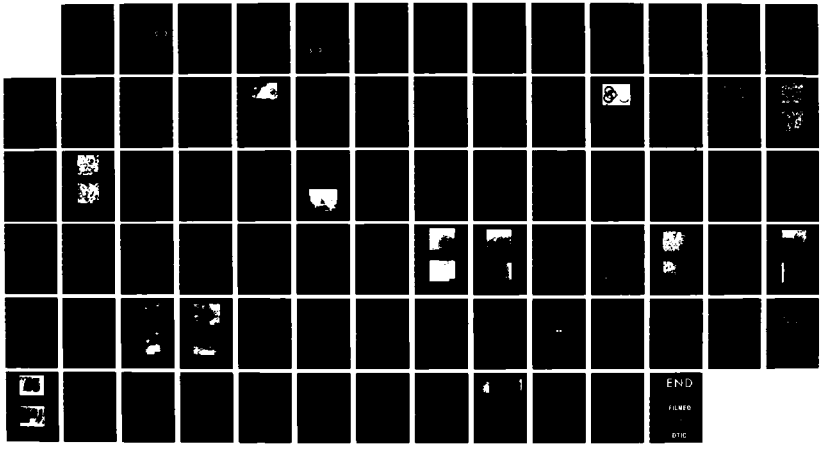

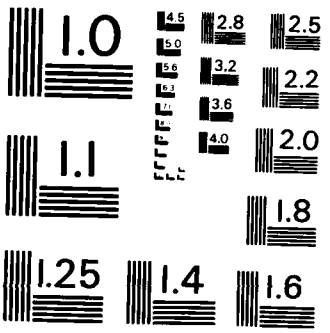

DEVELOPMENT OF SPACECRAFT MATERIALS AND STRUCTURES FUNDAMENTALS

S. Prochazka and S.L. Dole

FINAL SCIENTIFIC REPORT

Contract F49620-83-C-0101

Period Covered

June 1, 1984 - May 31, 1985

Submitted to

DIRECTORATE OF CHEMICAL AND ATMOSPHERIC SCIENCES
AIR FORCE OFFICE OF SCIENTIFIC RESEARCH
BOLLING AIR FORCE BASE, WASHINGTON, D.C. 20332

August 1985

APPROVED FOR PUBLIC RELEASE; DISTRIBUTION UNLIMITED

Prepared by

General Electric Company
Corporate Research and Development
Schenectady, New York 12301

SRD-85-021

unclassified

SECURITY CLASSIFICATION OF THIS PAGE

AD-A161 398

REPORT DOCUMENTATION PAGE

1a. REPORT SECURITY CLASSIFICATION: unclassified	1b. RESTRICTIVE MARKINGS
2a. SECURITY CLASSIFICATION AUTHORITY	3. DISTRIBUTION/AVAILABILITY OF REPORT: Approved for public release, distribution unlimited
2b. DECLASSIFICATION/DOWNGRADING SCHEDULE	
4. PERFORMING ORGANIZATION REPORT NUMBER(S): SRD85021	5. MONITORING ORGANIZATION REPORT NUMBER(S): AFOSR-[illegible]
6a. NAME OF PERFORMING ORGANIZATION: General Electric Company, Corporate Research and Development; 6b. OFFICE SYMBOL (If applicable)	7a. NAME OF MONITORING ORGANIZATION: Air Force Office of Scientific Research
6c. ADDRESS (City, State and ZIP Code): P.O. Box 8, Schenectady, NY 12301	7b. ADDRESS (City, State and ZIP Code): Bolling Air Force Base, DC 20332
8a. NAME OF FUNDING/SPONSORING ORGANIZATION: Air Force Office of Scientific Research; 8b. OFFICE SYMBOL (If applicable)	9. PROCUREMENT INSTRUMENT IDENTIFICATION NUMBER: F49620-83-C-0101
8c. ADDRESS (City, State and ZIP Code): Bolling Air Force Base, DC 20332	10. SOURCE OF FUNDING NOS. — PROGRAM ELEMENT NO.: 61102F; PROJECT NO.: 2303; TASK NO.: A3; WORK UNIT NO.:
11 TITLE (Include Security Classification): Development of Spacecraft Materials and Structures Fundamentals	
12. PERSONAL AUTHOR(S): S. Prochazka, S.L. Dole	
13a. TYPE OF REPORT: Final Scientific Report; 13b. TIME COVERED: FROM 6/1/84 TO 5/31/85	14. DATE OF REPORT (Yr., Mo., Day): Aug 31, 1985; 15. PAGE COUNT: 83
16. SUPPLEMENTARY NOTATION	
17 COSATI CODES — FIELD / GROUP / SUB. GR.	18. SUBJECT TERMS (Continue on reverse if necessary and identify by block number): Boron carbide, sintering, grain growth, microstructure, microcracking, mechanical properties, elastic modulus, mechanical oscillations, damping, strength

19. ABSTRACT (Continue on reverse if necessary and identify by block number)

Compacts of boron carbide powders with specific surface area $\geq 8\ m^2/g$ were sintered in argon at temperatures near 2200°C. Several of these powders were prepared by attrition milling of abrasive grade boron carbide. Densification to 95+% of theoretical density could be obtained only with compositions that had appropriate amounts of excess carbon. The microstructures were fine grained and uniform but underwent abnormal grain growth above 2235°C accompanied by transgranular microcracking. This grain growth could be inhibited by increasing the carbon content. Mechanical damping capacity was measured by the free beam and cantilevered beam techniques on boron carbide and other materials. Methods to enhance the damping capacity in a beam structure were analyzed. The flexural strength of sintered boron carbide was evaluated and related to powder processing and sintering parameters.

20 DISTRIBUTION/AVAILABILITY OF ABSTRACT: UNCLASSIFIED/UNLIMITED ☑ SAME AS RPT ☐ DTIC USERS ☐	21 ABSTRACT SECURITY CLASSIFICATION
22a. NAME OF RESPONSIBLE INDIVIDUAL: Dr Ulrich	22b TELEPHONE NUMBER (Include Area Code): (202) 767-4963; 22c OFFICE SYMBOL: NC

DD FORM 1473, 83 APR EDITION OF 1 JAN 73 IS OBSOLETE

unclassified

SECURITY CLASSIFICATION OF THIS PAGE

CONTENTS

ACKNOWLEDGMENTS

The research work reported here was conducted by the Physical Chemistry Laboratory of General Electric Corporate Research and Development under AFSC Contract F49620-83-C-0101. Dr. D.R. Ulrich of the Air Force Office of Scientific Research was Program Manager. Dr. S. Prochazka and S.L. Dole were principal investigators and the work was performed within the Ceramics Branch, Dr. R.A. Giddings, Manager.

The authors greatly appreciate the technical assistance of W.J. Dondalski, the electron microscopy work of N. Lewis and C. Joynson, and the X-ray diffraction work of C. Hejna.

STATEMENT OF THE TASK

Task I. Develop a detailed understanding of and procedures for the sintering of boron carbide.

Task II. Measure the mechanical damping capacity of boron carbide and evaluate means to enhance the damping capacity in structures consisting of inorganic materials. Additionally, evaluate the fracture strength and elastic modulus of sintered boron carbide and relate these to the characteristics of the sintered material.

SUMMARY OF RESULTS

1. Boron carbide of composition near B_4C shows minimal densification when fired at temperatures up to 2300 °C; typical densities are in the range 60 to 70% of theoretical density. The microstructure which develops in such material consists of an interconnected array of grains separated by large channeled pores. The major phenomenon in this microstructural development is the excessive growth of pores relative to grain growth and the failure to form appreciable necks between the grains. This failure apparently leads to a condition of thermodynamic pore stability and limited densification. Oxygen is an active species in this process.

2. Carbon additions to B_4C promote densification by inhibiting the pore growth process and allowing substantial necks between particles to form prior to densification. With 5 to 6 wt% added carbon (B/C atomic ratio $\leqslant$ 3.25) optimum densification is obtained. Firing in the temperature range 2220-2230°C produces sintered densities $\geqslant$ 97% of theoretical density with a fine-grained microstructure (grain size = 1 to 5 μm). Compositions containing less than the optimum carbon addition (2 wt% C) densify to 90% at higher temperatures (> 2250 °C), but this is attended and apparently facilitated by excessive grain growth. Solubility of the carbon in B_4C is < 1 wt% after cooling from the sintering temperature. No formation of a eutectic liquid is apparent and the sintering proceeds via solid state mechanisms.

3. At sintering temperatures above 2235 °C, abnormal grain growth occurs in carbon-doped B_4C by the formation of individual or clustered large grains (> 10 μm size). This growth is possibly induced by impurities such as Si, Al or Fe initially present in the B_4C material. Transgranular microcracking caused by the thermal expansion anisotropy of the B_4C crystals appears in coarse-grained structures when the grain dimensions approach 100 μm. Increased carbon additions (to 12 wt% C) inhibit the abnormal grain growth at

sintering temperatures up to 2270 °C without diminishing the sinterability of the B_4C.

4. Boron carbide powder with a specific surface area of about 8 m^2/g was required for densification of carbon-doped B_4C to 95% of theoretical density. Powders with surface areas of 2 m^2/g or less did not densify to over 80% density. Increasing the surface area to approximately 20 m^2/g provided at best only moderate increases in sinterability. An attrition milling process was used in this study to prepare sinterable B_4C powders (with surface areas of $\approx$ 8 to 20 m^2/g) from relatively coarse, abrasive grade B_4C material. The milling technique was efficient and introduced only minimal impurities to the powder.

5. The inherent mechanical damping capacity of B_4C was higher than that for many metals and ceramics, but does not qualify B_4C as a highly damped material. Attempts to achieve the objective of increased damping capacity by materials design techniques were not very successful. However, structural design techniques offered means to appreciably enhance damping capacity in structures containing high aspect ratio B_4C components, particularly with the introduction of specific damping elements to the structural assembly.

6. The flexural strength of sintered B_4C with appropriate powder processing and sintering conditions was approximately 550 MPa − 20% higher than that found for hot-pressed B_4C. A coarse-grained microstructure or the presence of carbon segregations in the microstructure was highly detrimental to the fracture strength of sintered B_4C.

I. INTRODUCTION

The development of structural members for a space vehicle apparatus is a question of the choice and development of materials and the selection of minimal compromise in design such that an optimum performance may be achieved. Given the generic application and the priorities for performance, materials have been identified that have potential beyond those presently in use or under consideration. To explore and ultimately realize this potential requires more data on properties and innovations in material processing that would allow evaluation of the benefits, feasibility, and cost.

Application

Large-aspect-ratio, electrically insulating structural components for long-term operation in the -200 °C to +200 °C range.

Materials Requirement

1. Chemical stability over the -200 °C to +200 °C range
2. Low density
3. Low outgassing
4. High stiffness
5. Electrically insulating but dielectrically lossy
6. High capacity for damping of mechanical oscillations of the completed structure
7. Low thermal expansion
8. Moderate thermal conductivity
9. Resistance to radiation

The above requirements led to the selection of boron carbide as an inert, high-potential candidate for such composite structures because the stiffness to weight ratio in B_4C exceeds any other substance (except Be metal). The feasibility of fabrication of complex structures from B_4C, however, has not been developed in the past and became the prime objective of this work along with an effort to find ways to meet the other criteria. In particular the aspect of the damping capacity in B_4C has not been studied at all and even general information on the damping of mechanical oscillations in ceramics has been scant. Therefore this subject became a separate task in this study.

In this report we discuss work performed between June 1, 1984 and May 30, 1985 in conjunction with the project "Development of Spacecraft Materials and Structures Fundamentals." The report is divided into two chapters: I) Sintering and Microstructure Development of Boron Carbide, and II) Mechanical Properties of Boron Carbide and Structures.

I. SINTERING AND MICROSTRUCTURE DEVELOPMENT OF BORON CARBIDE

A. Summary of Previous Work

Work performed during the first year of the contract period generated these significant results:[1]

1. Boron carbide (B_4C) powder compacts could be densified to > 95% of theoretical density (TD) with carbon additions in a manner similar to that reported by Schwetz and Grellner[2]. Compacts with no added carbon showed little densification; typical fired densities were 70% TD.

2. B_4C powders available from commercial sources were too coarse (surface area $\leqslant$ 2 m^2/g) for achieving sintered density over 90% TD. Attrition milling of selected powders was employed to increase the surface area to $\approx$ 8 m^2/g. Subsequently, the material could be sintered to high density with carbon additions.

3. Optimum sintering was achieved by firing at 2220-2230°C for 1/2 h in argon with a composition of B_4C plus 4-6 wt% carbon. Sintered compacts with 97% TD and a fine- grained ($\approx$ 3μm) microstructure were obtained.

4. At higher firing temperatures (> 2235°C) abnormal grain growth was observed, and this was sometimes accompanied by transgranular microcracking.

5. The feasibility of forming complex shapes of B_4C was demonstrated by extruding a B_4C powder-binder composition as high aspect ratio rods and subsequently firing these intact to high density.

For the most part, these results comprised a preliminary examination of the sintering behavior and microstructure development in sintered B_4C. The currently reported work provides a more detailed investigation into the sintering behavior of B_4C with attention given to

optimization of the process.

As noted, carbon additions were necessary to promote significant densification in B_4C. Other sintering aids have been reported,[15,16] but these most likely rely on the formation of second-phase liquids or compounds to induce densification. They also, in general, appear less reliable than the carbon sintering aid. Since carbon is a component of B_4C, its addition should not complicate any consideration of phase equilibria or sintering mechanisms. Because only a small addition of carbon is required, the properties of B_4C-C sintered compositions should be closely representative of B_4C itself. For these reasons, this work was solely directed at compositions in the B_4C-C system.

B. Material Source and Analysis

The initial steps in the sintering study were to identify and characterize suitable B_4C material. Available B_4C powders of reasonable purity were generally abrasive grade materials with a relatively coarse particle size (1 μm) and low specific surface area (< 2 m^2/g). These factors contributed to the inability to sinter (densify) these powders by the procedures used in this study. Attrition milling to reduce particle size was employed for selected powders to demonstrate the feasibility of producing sinterable B_4C from the abrasive grade powders. The procedures and results of the milling study are given in the next section.

One B_4C powder (ESK Grade 1500) was found which had a sufficiently fine particle size and high surface area (12 m^2/g)* for sintering. In the as-received condition, high levels of iron and titanium contaminants were present ($> 0.1\%$) in this powder. Consequently, a sulfuric acid leach was used as a purification step. This leaching step was applied to all B_4C powders used in this study.

Two other forms of the ESK material were also used. Grade 1200 was essentially identical

* After leaching

to Grade 1500 except that it had a coarser particle size and lower surface area (2.1 m^2/g). A high surface area material was obtained by sedimentation of the Grade 1500. This was accomplished by dispersing 200 g of powder in 5 l of water with 2.5 g of a dispersant.* The liquid suspension was allowed to settle for 22 h and then the upper 10 cm of a total 15 cm liquid height was siphoned off to collect the fine fraction of the powder. This was flocculated with nitric acid, decanted, washed with acetone and dried. Forty grams of fine powder was collected in this way and it had a surface area of 20.6 m^2/g.

Attrition milling was applied to three different B_4C powders – Norton Norbide, Aremco Superfine, and the ESK Grade 1500 – to produce additional sinterable B_4C. The Norton material contained considerable free carbon (5.2 wt%) in excess of the B_4C composition while the Aremco and ESK had less than 1 wt% excess carbon. All of the powders showed comparable X-ray diffraction (XRD) patterns and lattice parameters which correspond well with those reported for the composition B_4C.[3,4] Characteristics of all the B_4C powders as prepared for sintering are given in Tables 1 and 2. The analytical techniques are described in Appendix I. Sintering results given in this report are for the ESK Grade 1500 unless otherwise noted.

* Orozan, ITT Rayonier, Stamford, CT.

Table 1

B_4C POWDERS USED IN THE SINTERING STUDY

1. ESK Tetrabor Grade 1500, ESK, Tonawanda, NY. Leached with H_2SO_4.
2. ESK Grade 1500 attrition milled and leached with $H_2SO_4/HNO_3/HF$.
3. Norton Norbide, Norton Co., Worcester, MA. Attrition milled and leached with H_2SO_4/HCl.*
4. Aremco Superfine, Aremco HPM Division, Ossining, NY. Attrition milled and leached with $H_2SO_4/HNO_3/HF$.

* Attrition milling procedure for this material described in previous report[1]

Table 2

CHARACTERISTICS OF B_4C POWDERS

Powder	1	2	3	4
B/C atomic ratio	4.0	4.0	3.2	3.9
Oxygen (wt%)	1.15	1.10	0.68	1.63
Impurities (ppm)				
Ti	850	150	150	200
Si	700	800	800	700
Fe	300	200	1250	250
Ca	200	100	900	900
Al	5	100	70	300
N	1200	1200	1000	6700
Free carbon (wt%)	0	0	5.2	0.9
Median particle size (μm)	1.0	0.61	1.38	0.63
Specific surface area (m^2/gm)	12.0	17.5	8.8	18.5
XRD lattice parameters (Å)				
(Hexagonal)				
a_o	5.6016(12)	--	5.6038(9)	5.6022(10)
c_o	12.0744(25)	--	12.0789(19)	12.0815(21)

C. *Comminution of Boron Carbide*

Obtaining high densities in B_4C compacts by sintering is possible only with starting materials that have an average particle size in the one-micrometer range or less. In such powders, as in SiC, the fraction of particles $> 1\ \mu m$ and the size distribution determine the sinterability. To find a correlation between the particle size and the sintering response of B_4C, a fine powder preparation procedure was needed. In addition, any future application of the sintering process would require a reliable source of fine B_4C powders that would be most likely fabricated by comminution of coarser materials. The fine grinding of B_4C was therefore made an essential part of this development.

In previous comminution experiments[1] that were conducted in a ball mill and in an attritor, it was observed that the usual routine procedures failed to yield the required submicron particle size. The reason was the extreme abrasiveness of B_4C that resulted in so much iron wear on wet milling that after achieving a specific surface area of about 8 m^2/g, further particle size reduction practically ceased. In other words, the production of wear was limiting the achievable refinement. For instance, in a 1½ gal attritor on milling -325 mesh B_4C with 1/8 in. steel milling media, the wear of iron approached the weight of the charge after 8 h. The removal of this amount of iron from the product, although feasible, proved a very cumbersome and lengthy operation, making such a process impractical. Finer B_4C dispersions could then be prepared only in a few 10 g lots by Stoke's sedimentation of the acid leached product. A need for a new, more productive procedure was recognized and its development was undertaken.

There exists, of course, the option to synthesize B_4C by such a process in order to obtain a very fine dispersion directly. This has been, in fact, the preferred alternative in the fabrication of many other ceramics such as alumina, zirconia, or silicon carbide. Powders of B_4C

prepared by such commercial processes were sampled and tested previously;[1] however, their sintering behavior was not encouraging. To launch a parallel in-house program to synthesize B_4C with the right dispersion and properties was not possible because of funding constraints; it may be, however, a desirable avenue to pursue in future work.

In the search for a better comminution process, four different techniques were considered:

1. Milling with steel media with continuous magnetic removal of iron wear.
2. Attritor milling with B_4C active components.
3. The use of the turbomill developed and tested recently by the U.S. Bureau of Mines.[5]
4. Autogenous grindings in an attritor with plastic components and with B_4C grinding media.

Understandably, exhaustive studies could not be performed on all four techniques. Rather, the work served to identify the most promising and most easily adoptable technique under the circumstances and limitations of this program. The following discussion highlights the results and some problems encountered.

1. Continuous iron removal

Iron wear has been identified as the limiting factor in conventional milling of B_4C in an attritor, and, consequently, continuous magnetic separation of iron from a recirculating slurry was conceived as a possible improvement. To test the possibility, a gravity ferrofilter (S.G. Frantz, Trenton, NJ, model 41) was installed in the line that recirculated the slurry in the 1½ gal attritor (Union Process, Akron, Ohio, model S-1). The milling medium consisted of 1/8 in. steel balls and the charge was 1300 g of 1200 mesh B_4C. The formation of iron wear was, however, so massive that the ferrofilter plugged up in less than one minute of running time and the experimentation was discontinued. The difficulty arises from the design of the

iron separator that is built to remove small quantities of iron but is not suitable to handle large quantities.

2. Attritor components with B_4C

The concept of using mill liners and milling media of a composition approximately identical to that of the charge is quite popular in solving the wear problem in ceramic processing. It is, however, usually the solution of last resort because of increased expenses. The feasibility of this concept for milling silicon and silicon nitride was demonstrated recently by Herball, Glasgow, and Orth.[6]

In the present work we tested only the critical part, i.e., the agitator blades of a laboratory attritor (Netsch, Exton, PA, model 075). The 5 cm diameter blades, 0.8 cm thick were EDM-machined from a hot-pressed billet received from Ceradyne Company, Inc.

The assembled agitator is shown in Figure 1 after testing for 36 hours with a − 20 + 40 mesh grit of pre-rounded B_4C at 1500 rpm. The severe wear of the blades incurred in the relatively short test indicated that this approach was not practical for B_4C.

3. The U.S. Bureau of Mines turbomill

In a recent report Wittmer[5] described the development of the turbomill, a device designed for autogenous wet grinding of laboratory quantities of hard materials such as SiC. Additional work was reported by Hoyer and Petty.[7] This mill is composed of an inner-bladed cylindrical rotor and an outside bladed stator with a gap of 6 mm in between. These components are mounted coaxially in a jacketed cylindrical container. The rotor and stator were made either partially (blades only) or fully of ultra high molecular weight polyethylene (UHMW PE). The milling medium was a coarse fraction (− 20 + 36 mesh) of the same material as the charge to be ground. The mill was operated wet at about 1600-1700 rpm. Very good results are reported for milling of SiC that yielded a product with a specific surface area of 33 m^2/g.

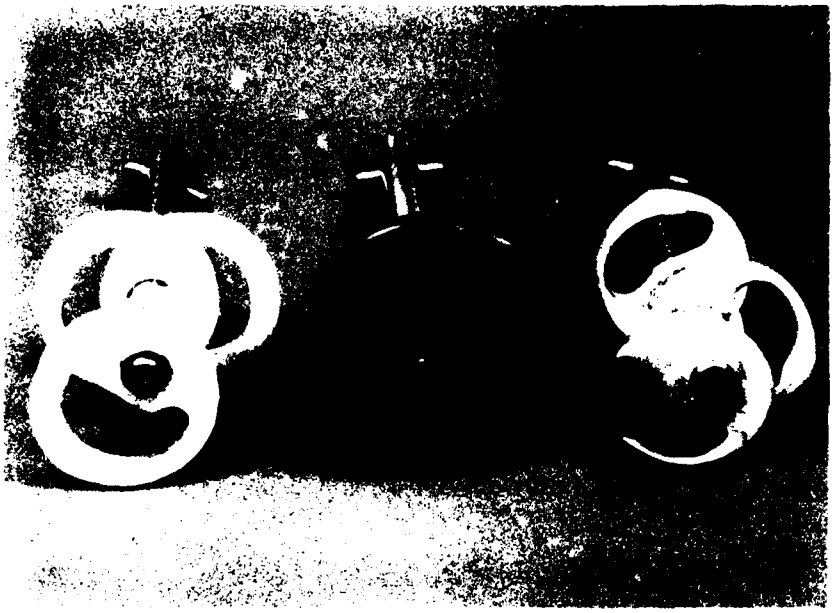

Figure 1. Attritor agitators with blades of polyethylene (left), hot-pressed B_4C, and alumina after a 36 h exposure to -20 +40 mesh B_4C grit at 1600 rpm

A duplicate of the Bureau's mill was built in this laboratory and subjected to several tests. Two runs were made with B_4C using the following charge:

1000 g	− 20 + 40 mesh prerounded* B_4C
330 g	1500 B_4C Tetrabor
1400 cc	Water
1 g	Orazon (sodium lignosulfonate) as dispersant
1430 rpm	
3 and 6 h running time	

The dispersion thickened considerably and additional deflocculant was used to control viscosity during the run. The slurry was then diluted, screened to remove the milling medi-

* Prerounding was done in a separate operation for 16 h in water.

um, and subjected to particle size analysis by screening down to 10 μm mesh size. A centrifugal particle size analyzer was used for analyzing the subsieve fraction. The results are shown in Table 3 and Figure 2.

The particle size analyses show substantial refinement of the subsieve fraction, particularly in the near 1 μm size of the distribution. This refinement was, however, not reflected in the specific surface areas of the product. The subsieve fraction gave 8.2 m^2/g (actually a decrease) after 3 h and 10.75 m^2/g after 6 h milling, only a moderate increase from the initial 9.2 m^2/g for the Tetrabor 1500 charge. This is probably the consequence of two effects. First, because deagglomeration took place due to the high shear forces with only little fragmentation in the submicron range, the decrease of the median particle size is not accompanied by a specific surface area increase. Second, the coarse fraction used as milling medium is being broken up, as evidenced in the sieve analysis in Table 3. The data shows that 12% of the coarse grit disintegrated in 6 h. The size distribution indicates that the rate of particle removal is inversely proportional to particle size; i.e. the smaller the particle, the higher the

Table 3
SIEVE ANALYSIS

Sieve No.	Particle Size Interval, μm	Weight of Oversize, g	Cumulative Weight of Oversize, g
20	840	0	
-20 +40	840-240	880	880
-40 +100	420-250	46	926
-100 +200	250 75	17	943
-200 +400	75 37	2.9	945.9
-400 +10 μm	37 10	1.1	947.0

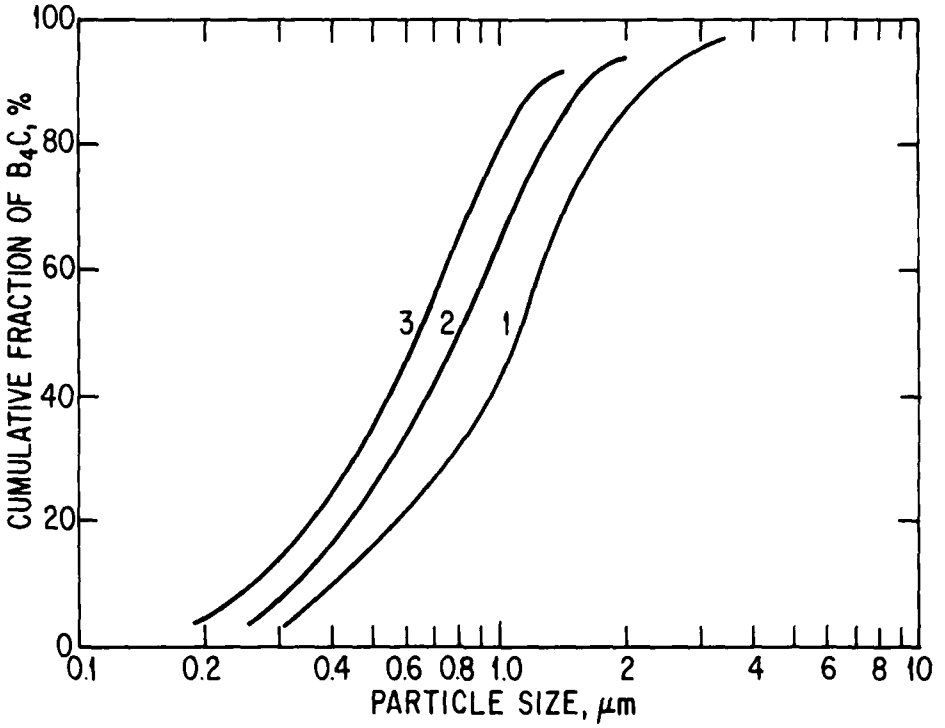

Figure 2. Particle size distribution of B_4C, Tetrabor 1500 as received (1), and after 3 (2) and 6 h (3) milling in the turbomill

probability it will be broken up. However, because this relationship does not apply any longer in the submicron size range, the turbomill rapidly produces particles near 1 μm but has only limited effect in the range of 0.5 μm. The drop in the specific surface area can be well understood in this way. The results of Hoyer and Petty obtained with several hard materials seem to agree with this explanation.[7]

The turbomill is an impressive innovation because its use solves the problem of wear/contamination on fine grinding of hard materials. It is effective in refining materials down to the micron size range; however, in its present version it has only a small effect in producing particles in the tenth of a micron range. Further modifications and optimization are needed to achieve this.

4. Autogenous grinding in the attritor

The principle of autogenous grinding and the use of UHMW PE active components introduced by the Bureau of Mines' investigators were applied with promising results to submicron grindings in the laboratory attritor (Netsch Co. model 075). The blades of the agitator were made of UHMW PE, and the jar was lined with regular PE. Prerounded − 20 + 40 mesh B_4C grit served as the milling medium. The mill was run at 1600 rpm and different liquids were used in a series of experiments. The results of several runs are summarized in Table 4 and Figures 3 and 4, and are discussed below.

Effective particle size reduction of B_4C in the submicron range was obtained. This is shown by the specific surface areas before and after milling and by the particle size distribution curves. The particle size reduction continued up to 24 h of milling, the longest time applied. It was shown with other materials that refinement continued still at 65 h grinding time, although at a reduced rate.[8] Using a deflocculant was essential to control the rapidly increasing viscosity of the slurry that resulted from the production of very fine particulates. In alcohol, the viscosity increase was small and no deflocculant was needed.

The disintegration of the milling medium was small as shown by the oversize fractions on sieves mesh 400 and 10 μm in experiments 1, 2, 3, and 6. The large oversize fraction in experiments 4 and 5 was the result of the coarseness of the charge of the Aremco B_4C, in which case the largest particles of the charge were not broken up. In order to obtain comminution, the size ratio of the milling medium and the largest particles of the charge has to be 10 or more. Since this was not the case in experiments 4 and 5, a part of the charge remained unmilled.

The wear of the agitator PE blades was, in general, surprisingly small. Figures 1 and 5 show agitators with blades of PE, B_4C, stellite, and alumina after comparable exposure. The

Table 4

RESULTS OF AUTOGENOUS MILLING IN ATTRITOR 075

	Charge	Spec. Surface Area m^2/g	Medium	Deflocullant	Time h	Residue on Sieve, g −40 +200	−200 +400	−400 +10 μm	Spec. Surface Area m^2/g	Median Particle Size, μm	% <1 μm	Fig.
1	100 g B_4C 1500, ESK	9.2	ethanol	none	8	—	1.1	0.4	17.5	0.61	73	3
2	100 g B_4C 1200, ESK	3.0	ethanol	none	9	—	0.6	0.2	17.5	0.58	75	—
3	95 g B_4C 1500, ESK	9.2	water	DAXAD *	22	—	0.76	0.35	28.6 **	0.48	87	3
4	100 g B_4C Aremco −200 mesh	—	water	DAXAD *	23	24.8	0.8	0.4	23.0 ***	—	—	—
5	100 g B_4C Aremco −200 mesh	—	N-Heptane	Oleic ac. Bees wax	24	11.2	1.6	—	18.5	0.63	84	4
6	100 g B_4C 1500, ESK	10.8	N-Heptane	Oleic ac. Bees wax	22	—	0.6	—	19.5	0.55	88	4

* Daxad, W.R. Grace, Co., Lexington, Mass.

** The surface area after leaching in dilute H_2SO_4 dropped to 23.5 m^2/g

*** The surface area after leaching in dilute H_2SO_4 dropped to 13.5 m^2/g

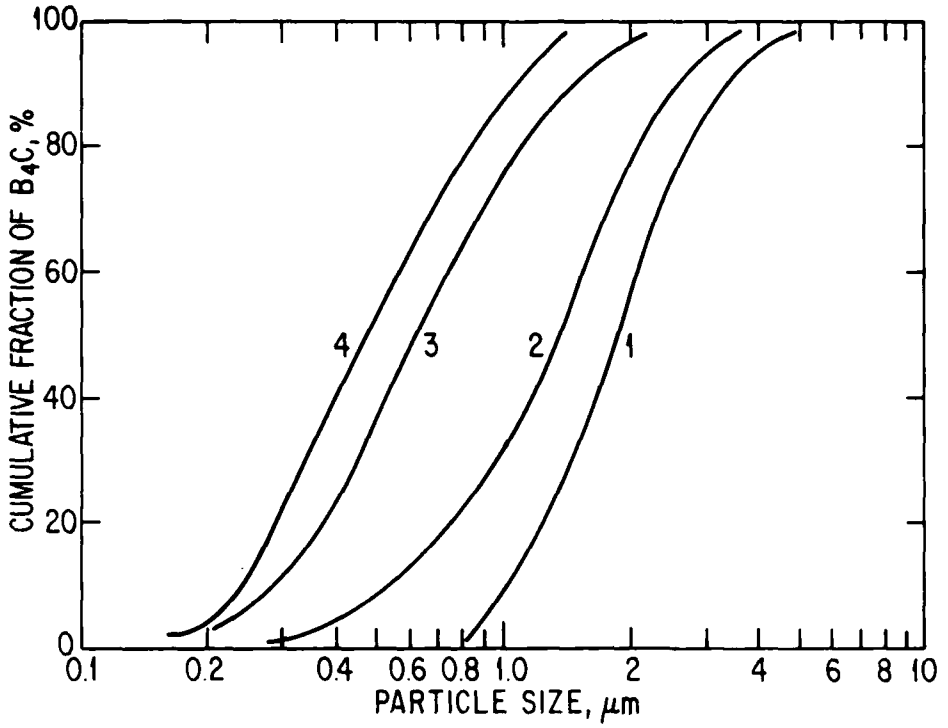

Figure 3. Particle size distribution of Tetrabor 1200 (1), Tetrabor 1500 (2), and Tetrabor 1500 milled 8 and 22 h (3), (4) in the laboratory attritor.

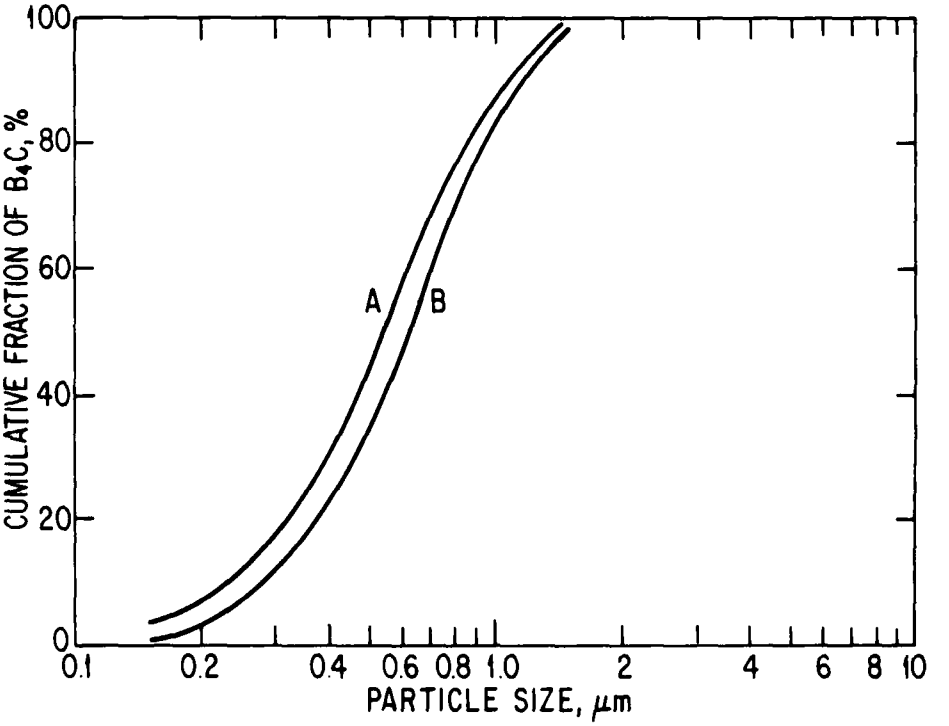

Figure 4. Particle size distribution of Tetrabor 1500 (A) and Aremco -200 mesh (B) after 22 h and 24 h milling in the attritor. See table.

Figure 5. Attritor agitator of stellite (left) and UHMW PE after about 50 h exposure to *-20 +40 mesh B_4C grit at 1600 rpm*

wear of the PE blades is estimated to be a factor of 5 to 50 less than that of the other tested materials. The wear was determined quantitatively in run no. 2 and amounted to 2.1 wt% of the charge. This was the sum of the weight loss of the blades and the lining as a percent of the weight of the charge of the fines. It was observed, however, that the wear depended on other factors, especially on the particle size of the charge, viscosity of the slurry, temperature, the chemical nature of the liquid, and the rate of spinning. The wear increased in runs 4 and 5 where a relatively coarse charge was used. It was also larger in run 6 compared to run 2, probably due to the chemical effect of heptane.

The wear of the PE lining was minimal and could not be accurately evaluated because copious particles of B_4C were embedded in the lining. It is possible that the embedded particles play a role in the unexpected wear resistance of the plastic components.

Analyses of the milled B_4C showed pick-up of a few tenths of a percent each of Si, Fe, and W. The tungsten was traced to accidental contamination that resulted from the use of the attritor for tungsten processing in another program. The iron originated from the preferential breakup of some undetermined iron compound present in the coarse B_4C fraction used as the milling medium. Since the compound was not magnetic, it could not be removed. The source of silicon was not positively identified; it may have been from a source similar to the iron. The impurities were removed by leaching with dilute H_2SO_4 and HF from the product.

In summary, the autogenous grinding in the modified attritor was by far the most successful procedure for comminution of B_4C to submicron dispersions. The two critical aspects of the process, the wear and the production of intermediate particle sizes 1-10 μm by the breakup of the milling medium, were acceptable. The contamination is certainly manageable by additional improvements.

D. Microstructure Development in B_4C Prior to Densification

Compacts of fine boron carbide powders with composition close to B_4C showed little tendency to densify at firing temperatures up to 2300°C. Densities of 60-70% TD were typical. The structure that develops in this material during firing is characterized by a highly porous, interconnected structure with clusters of grains connected by small necks and separated by large, channeled porosity. Photomicrographs of a fracture section (Figure 6) and a polished section (Figure 7) show this quite clearly. Similar structure development has been noted for "unsinterable" powder compacts of silicon and silicon carbide.[9]

Compacts of B_4C (Figure 8) and B_4C + 6 wt% C (Figure 9) fired at 2000°C in an argon atmosphere* for 30 min show strikingly different structures even though neither compact has

* All firing was done in an argon atmosphere in a graphite furnace with a 30-min hold at temperature.

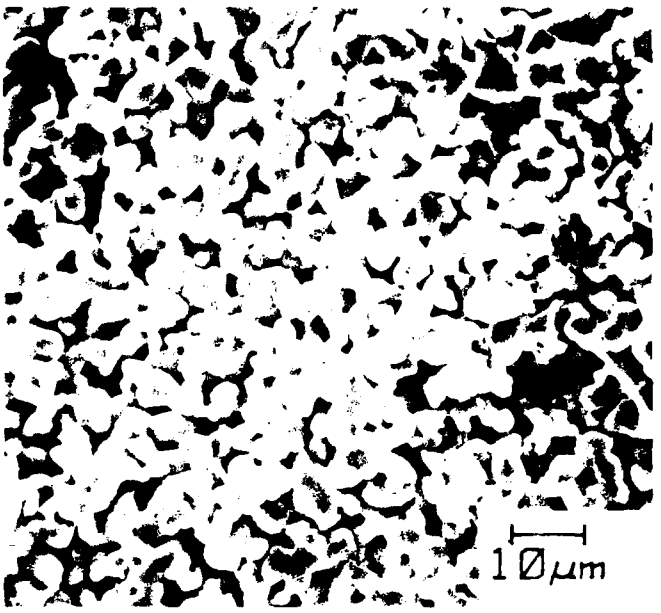

Figure 6. SEM micrograph of fracture surface of B_4C fired at 2250 °C for 30 min in argon

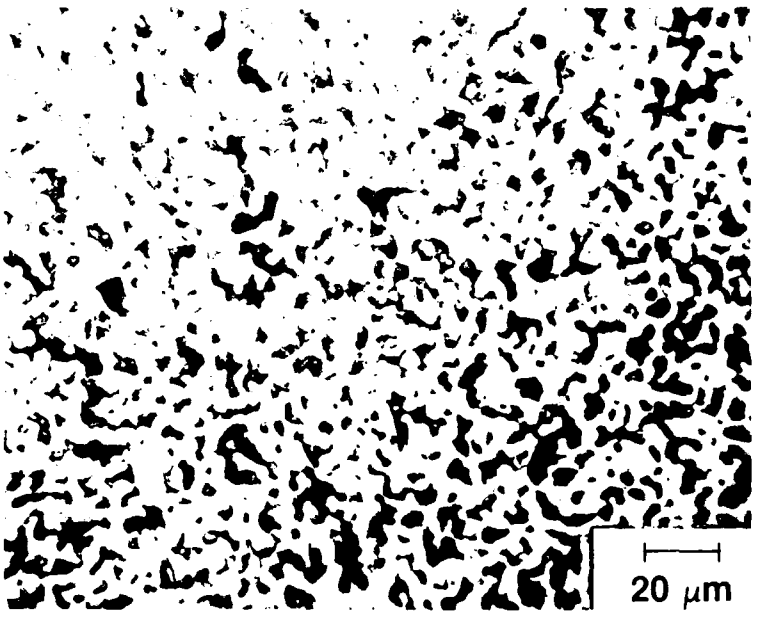

Figure 7. Polished section of B_4C fired at 2250 °C for 30 min in argon.

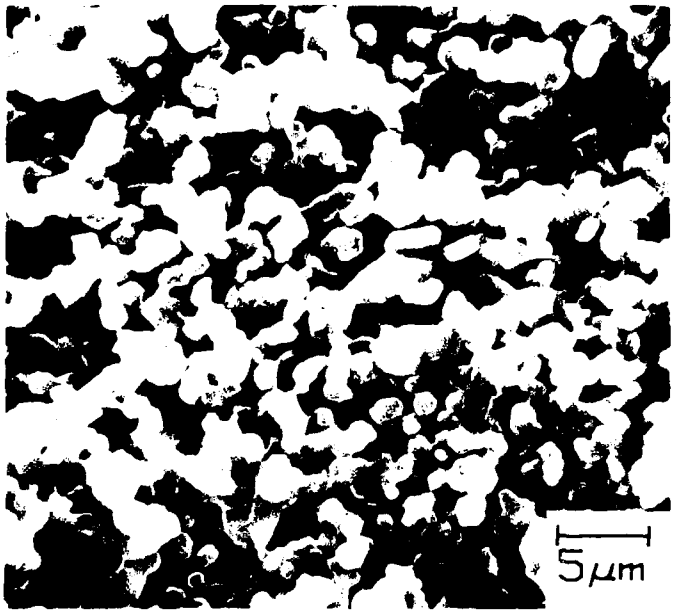

Figure 8. SEM micrograph of fracture surface of B_4C fired at 2000 °C for 30 min in argon

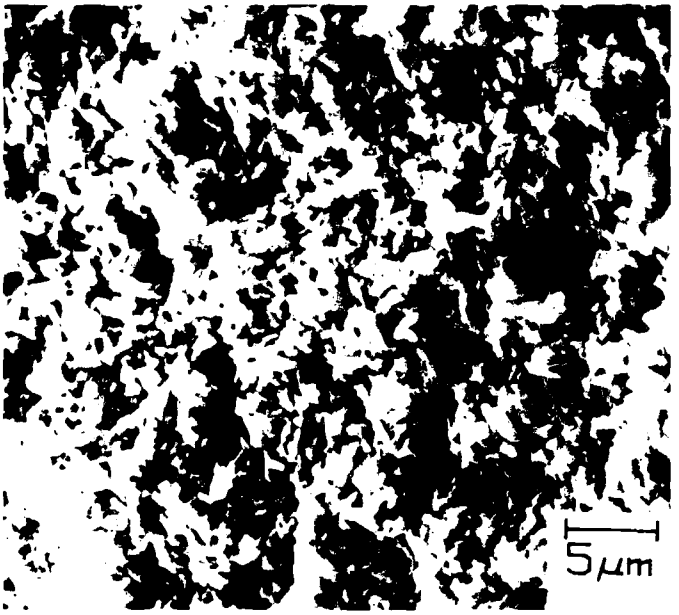

Figure 9. SEM micrograph of fracture surface of B_4C + 6 wt% C fired at 2000 °C for 30 min in argon

densified to any great extent (densities < 70% TD). The fired compact without carbon addition has a structure similar to that in Fig. 6; the only difference is that the pore-grain structure is about two times finer in scale. It is apparent that significant surface-to-surface mass transport has occurred, resulting in pore growth and rounding of the grains.

The sample with 6 wt% carbon exhibits a finer structure with edged grains and a considerably smaller pore size to grain size ratio. In many instances, the particles have sintered together into blocks, indicating that substantial neck growth has occurred between particles. The carbon addition has inhibited the surface-to-surface mass transport mechanism responsible for pore growth and rounding of grains. Upon firing at a higher temperature, this material will undergo substantial densification, in contrast to the B_4C with no carbon addition, which will experience only limited densification.

Figures 10 and 11 compare an as-pressed compact of undoped B_4C and one fired at 1500 °C for 30 min. Obviously, the pore growth and grain morphological changes are active even at 1500 °C. The pressed compact consists of very fine pores and has a broad distribution of particle sizes. After firing at 1500 °C, the pores have grown and many of the finer particles have disappeared. In B_4C with or without carbon additions the finer particles are eliminated during firing at elevated temperatures. This is attended by pore growth in undoped B_4C and by particle neck growth in carbon-doped B_4C.

To characterize this structure development, surface area and pore size (porosimetry) analyses were used to determine the course of events in B_4C compacts prior to any densification. Results are listed in Table 5. A large (50%) decrease in surface area may be realized at 1250 °C, well below the temperature range where any densification proceeds. The surface area decreases with increasing temperature, regardless of any carbon addition, and correlates well with the pore growth in the undoped B_4C. The major effect of the carbon addition is illustrat-

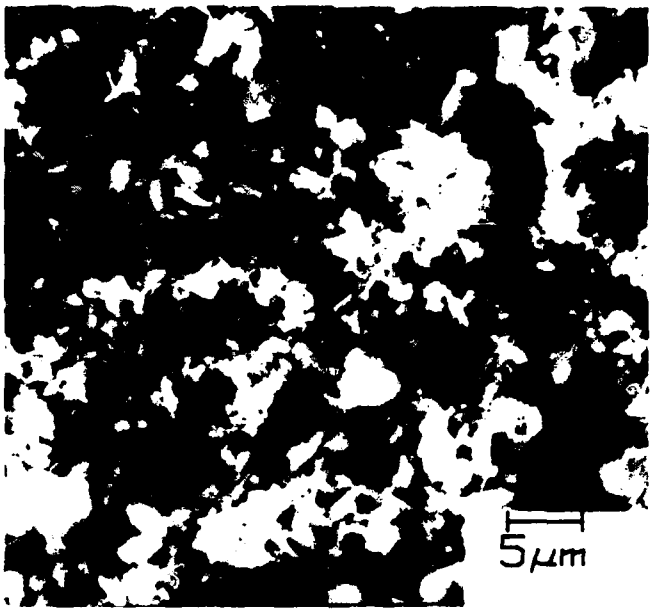

Figure 10. **SEM micrograph of fracture surface of an as-pressed B_4C compact.**

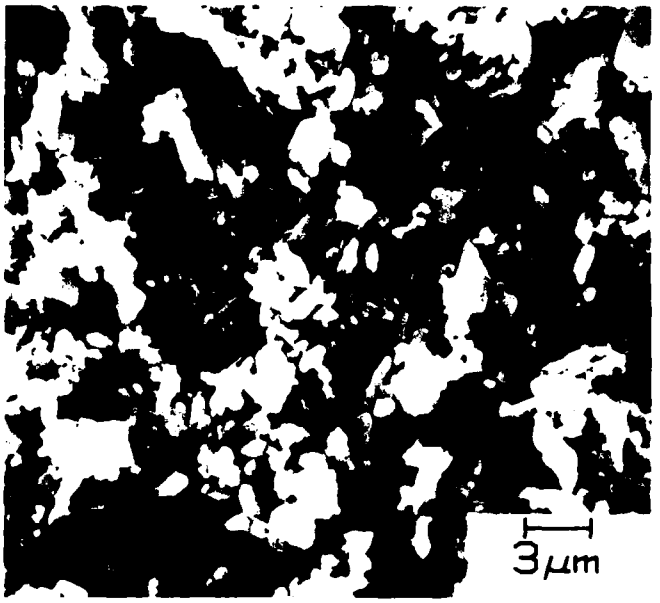

Figure 11. **SEM micrograph of fracture surface of B_4C fired at 1500 °C for 30 min in argon**

Table 5

SURFACE AREA AND POROSIMETRY ANALYSIS FOR B_4C COMPACTS ANNEALED AT VARIOUS TEMPERATURES

	Composition			
	B_4C		B_4C + 6 wt%C	
Anneal Temperature (°C)	Surface Area (m^2/g)	Median Pore Size (μm)	Surface Area (m^2/g)	Median Pore Size (μm)
initial	12	0.14	12	--
1250	6	--	--	--
1500	3.4	0.36	5.3	--
1750	2.8	0.47	4.7	--
2000	1.4	0.77	3.3	0.24
2250	--	1.39	(compact densifies)	

ed by the pore size measurement for the compacts annealed at 2000 °C. The compact with the carbon addition has a median pore size three times finer than its counterpart with no carbon addition, and, likewise, the surface areas are different. At all of the annealing temperatures, the surface area for carbon-doped material is higher than that for undoped material, indicating that carbon is inhibiting the surface-to-surface mass transport which yields surface area loss and pore growth. This leads to the conclusion that the carbon addition plays an important role in microstructure development prior to densification and has a profound effect on the eventual sinterability of the material.

To fully understand the mechanistic role of carbon in this system, considerably more study is required. However, it can be surmised that oxygen may contribute strongly to microstructure development in B_4C since it is present in both the starting material and the firing

atmosphere (argon with ≈ 10 ppm O_2). Oxides of boron (B_2O_3 and BO) can form, and these have sufficiently high vapor pressures (> 10^{-6} atm) above 1250 °C to possibly contribute to the surface-to-surface transport, leading to the observed microstructural changes in undoped B_4C. Excess free carbon in B_4C will react with the oxygen, and thus the role of carbon may simply be to remove oxygen or to limit its activity.

This assumption was tested by annealing compacts of undoped B_4C at 1500 °C in closed graphite crucibles in atmospheres of different oxygen content. A low oxygen content atmosphere was induced by inserting a strong oxygen getterer (yttrium carbide, YC_2) in the crucible but not in contact with the compact. Similarly, a high oxygen content atmosphere was provided by adding boric oxide to the crucible. Surface area and pore size results for the annealed compacts are given in Table 6. Obviously the presence of oxygen enhances pore growth and surface area reduction.

A further experiment was conducted where compacts of B_4C and B_4C with 6 wt% carbon were annealed at 1500 and 1750 °C and the oxygen content of the annealed compacts was determined. Results are listed in Table 7. Much of the oxygen is removed simply by anneal-

Table 6

SURFACE AREA AND POROSIMETRY ANALYSIS FOR B_4C COMPACTS WITH VARYING ATMOSPHERIC OXYGEN CONTACT

Compacts annealed in flowing argon for 30 min at 1500 °C

Atmospheric Control Addition	Surface Area (m^2/g)	Median Pore Size (μm)
none	3.4	0.36
YC_2 (low oxygen)	4.4	0.22
B_2O_3 (high oxygen)	1.9	0.61

Table 7

OXYGEN CONTENT OF B_4C COMPACTS ANNEALED AT 1500 °C OR 1750 °C FOR 30 MINUTES IN ARGON

Composition	Anneal Temperature (°C)	wt% Oxygen
B_4C	initial	1.15
B_4C	1500	0.43
B_4C	1750	0.40
B_4C + 6 wt% C	1500	0.39
B_4C + 6 wt% C	1750	0.20

ing at these temperatures, but with added carbon the oxygen content in the B_4C compact is lower relative to that in the undoped compact.

It appears to be a reasonable assumption that oxygen is an active species in B_4C at elevated temperatures and contributes to microstructural development in "unsinterable" compacts of B_4C. Further, it appears that carbon intimately mixed with the B_4C inhibits this process by removing or deactivating the oxygen in the vicinity of B_4C particle surfaces.

From the results discussed in this section, a reasonable outline of the sintering process in B_4C can be defined. In the absence of excess carbon, a B_4C compact when fired undergoes significant surface-to-surface mass transport, which produces growth of pores and rounding of particles. This occurs at fairly low temperatures ($\leqslant$ 1500 °C) and coincides with large reductions in surface area. Oxygen present in the B_4C or in the firing atmosphere facilitates this process, possibly through the formation of volatile oxides of boron. As a sufficiently high temperature for densification is approached ($>$ 2000 °C) the microstructure consists of interconnected grains surrounded by channeled porosity, and this structure persists while very little densification occurs at temperatures up to 2300 °C.

With appropriate carbon additions, a B_4C compact undergoes surface area reduction at elevated temperatures, but substantially less pore growth and more particle-particle neck growth occur. The carbon prevents significant pore growth and particle rounding by inhibiting the surface-to-surface mass transport active in undoped B_4C. Most likely carbon achieves this by suppressing the activity of oxygen in the system. At the sintering temperature, B_4C compacts with this structural development readily densify.

The pore growth process is perhaps the critical feature influencing the sinterability of B_4C. The basis for this conclusion lies in the arguments presented by Kingery and Francois[10] and later by Prochazka[11] in his study of sintering silicon carbide. Briefly, it is predicted that if the grain size to pore size ratio in a sintering compact is small enough (i.e., pores are large), then pores may become thermodynamically stable and will tend not to shrink during firing; hence, densification ceases. The dihedral angle formed by the pore-grain boundary junction is important, and pore stability is favored by a small dihedral angle. From TEM micrographs (such as Figure 12) it was observed that the dihedral angle in B_4C, while not constant, tended to be

Figure 12. TEM micrograph of residual pore in B_4C fired at 2250 °C

$\leqslant 90°$. This is comparable to the dihedral angle observed in uranium dioxide[10] and silicon carbide,[12] which are difficult to sinter without appropriate sintering aids or conditions. In a readily sinterable ceramic material, such as aluminum oxide, the dihedral angle is typically well above 100°.[10] The presence of very faceted pores (that is, pores with nearly flat surfaces) in fired B_4C was a good indication that pore stability had been achieved. This was also true for residual pores in sintered carbon doped B_4C. The kinetics of the pore growth process may thus lead to a condition of pore stability. In undoped B_4C, grain growth is much less than pore growth, so that a small grain size to pore size ratio results which favors pore stability and not densification. The effectiveness of carbon as a sintering aid is manifested by its ability to inhibit the pore growth, thereby producing a microstructure with a relatively high grain size to pore size ratio (fine pores), which is conducive to densification. The carbon may also contribute to densification kinetics in other ways at the sintering temperature, but this could not be readily determined in this study.

E. Sintering Results for B_4C-C Compositions

To fully characterize the sintering of the carbon-doped B_4C, it was necessary to examine a number of parameters. These are listed below and each is considered separately.

1. Method of carbon addition
2. Compaction pressure
3. Particle size and surface area of starting powder
4. Amount of carbon addition
5. Firing temperature
6. Impurities

The standard sintering process for B_4C was as follows. Powder compacts were die-pressed and then placed in closed graphite crucibles. Firing was carried out in a graphite resistance element furnace with a flowing argon atmosphere (0.5 l/min). The temperature was raised at an approximate rate of 25°C per minute to the peak temperature, which was maintained for 30 min. Occasionally, compacts were fired without crucible containment, with no effect on the results. The sintering temperatures given are +/- 5 °C unless a temperature range is specified. Temperature was measured with an optical pyrometer sighting directly on the crucible or compact.

1. Method of carbon addition

The procedure for preparing powders for sintering followed a fairly standard format. However, the form of the carbon addition to the B_4C powder was critical to the eventual sintered density. The addition was made in one of several forms:

a. A thermoset resin* in a solution with methanol.

b. The thermoset resin as an emulsion in a mixture of water and methanol.

c. Monarch carbon (surface area = 100 m^2/g).

d. Sterling carbon (surface area = 10 m^2/g).

e. Graphite powder (−325 mesh)

In each case, the additions were wet mixed with the B_4C powder as a slurry with methanol on a vibratory mill for 30 min, then dried and screened through a 40-mesh sieve. In resin based compositions, the resin was sufficient as a pressing binder. The other compositions required the addition of 4 wt% carbowax as a pressing binder.

* Either Novolac 31720, Durez, Tonowanda, NY, or Resin 6877, Schenectady Chemicals, Schenectady, NY.

In principle, the addition of the resin was the most attractive form of carbon since it acted initially as a binder and during firing decomposed to 50% by weight carbon. When added as a solution, the resin should mix intimately with and coat B_4C powder particles. A major drawback, however, was that during drying some of the resin segregated as the solvent was removed, producing hard, gritty agglomerates in the powder. These agglomerates had serious implications on the fracture strength of sintered B_4C as is discussed later. The other forms of carbon addition, including the resin- emulsion, produced finely divided powders.

Two variations of the resin-solution powder were investigated as means to eliminate the agglomerates. The first involved "charring" the powder at 400 °C in argon to decompose the resin to carbon powder. The second involved a wet-milling step to break up the agglomerates and redistribute the segregated resin. This was accomplished by vibro-milling the powder in a polyethylene bottle with heptane and teflon-coated stirring bars for 10 to 18 h. Other milling media, such as tungsten carbide, were not used so as to avoid contamination of the B_4C. Since the resin was insoluble in heptane, segregations of resin did not re-occur upon drying of the milled powder, and a finely divided material was obtained.

Compacts of the various powders were die-pressed and then sintered at 2220-2230 °C to determine the effect of the carbon addition technique. In some cases the dried powders were ground with a mortar and pestle and screened through progressively finer mesh sieves prior to pressing. Different compaction pressures were also employed. All compositions were B_4C + 6 wt% carbon.

Representative sintered density values are given in Table 8 for the different powders. Consistent sintered densities greater than 95% TD were obtained only for compacts of powder with the resin-solution addition. Results for the other powders were generally inconsistent, but typically the sintered density was less than 95%. The charred powder also gave inconsistent results, but densities above 95% were possible. Screening any of the powders through

Table 8

EFFECT OF CARBON ADDITION TECHNIQUE ON SINTERED DENSITY FOR COMPOSITION B_4C + 6 wt% C

Sintered in argon at 2200-2230 °C for 30 min

Additive Type	(mesh size)	Compaction (MPa)	Sintered (g/cm)*	%TD
monarch carbon	-40	370	2.21	88.1
monarch carbon	-40	620	2.25	89.7
monarch carbon	-325	620	2.35	93.9
monarch carbon	-325	830	2.37	94.8
sterling carbon	-150	370	2.26	90.4
sterling carbon	-325	370	2.34	93.4
graphite	-150	370	2.22	88.7
graphite	-150	620	2.26	90.4
resin emulsion	-400	370	2.35	93.9
resin emulsion	-400	370	2.37	94.8
charred resin	-40	370	2.38	94.9
charred resin	-40	370	2.42	96.5
resin solution	-40	370	2.42	96.6
resin solution	-150	370	2.44	97.3
resin solution	-150	370	2.44	97.4
resin solution	-325	370	2.45	97.7
resin solution	wet milled	370	2.46	98.2

* Sintered densities are corrected for the amount of carbon added.

the finer mesh sieves or using higher compaction pressures tended to improve sintered density. The best densities were obtained from resin-solution powders that had been wet milled in heptane prior to compaction.

The most likely reason for the variation in sintered density lies with the degree of carbon distribution in the B_4C powder. The most complete distribution would be expected with the resin-solution addition where the resin could coat B_4C particles. This is indicated by the higher sintered densities for this powder. The other powders relied on particle-particle mixing, which apparently is less complete and leads to lower and more inconsistent sintered density. Graphite additions generally produced the lowest sintered density, suggesting that the type of carbon (crystalline graphite vs. amorphous carbon) may also be an important factor. The fact that the "charred" powder yielded intermediate results indicates that some of the benefit of the resin-solution addition is lost if the resin is decomposed prior to compaction.

Grinding and screening the powders to finer mesh sizes usually improved sintered density for all the powders, but was generally most effective for powders which otherwise would not densify well. This process probably improves the carbon distribution and removes the agglomerates in the resin-solution powder, thereby improving the densification behavior. The best sintered densities were obtained with resin-solution powders that were milled in heptane to remove agglomerates and redistribute segregated resin. Thus the optimum powder preparation involved adding carbon as a resin solution and subsequently milling several hours in heptane prior to compaction. This process was used for preparing powders for most of the further sintering experiments.

2. Compaction pressure

The effect of compaction pressure on sintered density was evaluated in two separate experiments. In the first, powder with the resin-solution addition of composition B_4C + 6 wt%

carbon was pressed in a 3/8 in. diameter steel die at various loads. The compacts were sintered at 2220-2230 °C. In the second experiment the same powder composition was "charred" at 400 °C in argon and compacts pressed at various loads and sintered as above. The sintering results are given in Table 9.

Table 9

EFFECT OF COMPACTION PRESSURE ON SINTERED DENSITY

Powder: B_4C + 6 wt% C (resin-solution addition) with no wet milling.
Sintered in argon at 2220-2230 °C for 30 min

Compaction Pressure (MPa)	Sintered Density (g/cm^3)	% TD
185	2.31	92.2
250	2.35	94.1
310	2.36	94.2
370	2.39	95.3
430	2.41	96.4
500	2.40	96.0

Powder: same as above except powder "charred" at 400 °C in argon prior to compaction.

Compaction Pressure (MPa)	Green Density (g/cm^2)	Sintered Density (g/cm^2)	% TD
185	1.15	2.18	87.1
370	1.24	2.24	89.6
620	1.29	2.29	91.6
930	1.37	2.33	93.2

It is obvious from the data that increasing compaction pressure increases the sintered density. This effect introduced an additional variable to the sintering experiments. To normalize, later compacts were conventionally pressed at a 4500 kg load in the 3/8 in. die (620 MPa). This was a preferred choice for compaction pressure since the sintered density for resin-solution powders appears to maximize above the 370 MPa pressure level. Typically, the green density of compacts pressed at 370 MPa or higher was 1.42 g/cm^3 (56% TD referred to theoretical density of B_4C = 2.52) with the correction made to eliminate the mass of the added resin. The influence of compaction pressure may also have contributed to the inconsistencies and certainly to the improvements in sintered density for powders with the carbon or graphite powder additions.

The improvement in sintered density is probably due to the formation of more particle-particle contacts as the packing efficiency improves with increasing compaction pressure. Consequently, the population of large pores and the overall average pore size may be decreased. Sufficiently large pores initially present in the powder compact may become stable by the means discussed earlier and remain as residual porosity in the sintered compact. Their elimination allows higher sintered density to be obtained.

3. Particle size and specific surface area

It is common in ceramic systems that as the average particle size of a given powder decreases (and consequently its specific surface area increases), the sinterability of the powder increases. In other words, a higher sintered density may be obtained for a given firing temperature or a given density may be obtained at a lower firing temperature for a finer powder. There will inevitably be an upper limit on particle size where appreciable sintering will not occur. It was of interest to determine what particle size was required for sintering B_4C and to what extent, if any, further particle size reduction would benefit the sintering process.

Since the B_4C powders contain a distribution of particle sizes, the specific surface area of the powders was utilized as a measure of the degree of powder fineness. For the experiments the available ESK B_4C powders were used, as they had essentially the same composition. They were Grade 1200 (surface area = 2.1 m^2/g), Grade 1500 (surface area = 12 m^2/g) and the sedimented fine fraction of Grade 1500 (surface area = 20.6 m^2/g). To each powder 6 wt% carbon was added in the form of the resin solution, followed by wet milling in heptane. Compacts were die-pressed and sintered at temperatures between 2100 and 2250 °C. The sintered density results are shown in Table 10.

The low surface area powder (Grade 1200) exhibited no significant densification. Previously it was found that a surface area of $\approx$ 8 m^2/g was sufficient for densification to 95% TD. In addition, Schwetz and Grellner[2] found that a B_4C powder with a surface area of 5.2 m^2/g was marginal. Thus, it is apparent that some minimum surface area near 8 m^2/g is needed to accommodate densification in carbon doped B_4C to 95% TD.

The highest surface area B_4C (sedimented powder) yielded sintered densities moderately better than the Grade 1500 at firing temperatures up to 2200 °C. At 2250 °C, the two powders arrive at approximately the same density. The benefit of increased surface area does not appear to be great; in fact, the powder processing may be a more important factor. As shown in Table 10 for the Grade 1500, increasing the duration of the wet-milling step improves the sintered density so that it approaches the values achieved with the sedimented powder.

4. Amount of carbon addition

B_4C powder compacts without added carbon would not densify beyond 70% TD. Only the attrition-milled Norton B_4C which contained much excess carbon showed appreciable densification. However, this excess carbon was in the form of graphite, a marginal sintering

Table 10

SINTERED DENSITY FOR B_4C POWDERS OF VARYING SURFACE AREA

Composition is B_4C + 6 wt% C (resin-solution addition); wet milled 18 h, except (*) for 10 h. Sintered in argon with a 30-min hold at temperature.

Powder	Surface Area (m^2/g	Sintering Temperature °C	Sintered Density (g/cm^2)	Sintered %TD
Grade 1200	2.1	2250	1.88	75.0
Grade 1500(*)	12.0	2100	2.09	83.3
Grade 1500(*)		2150	2.27	90.8
Grade 1500		2150	2.35	93.8
Grade 1500(*)		2200	2.40	95.8
Grade 1500		2200	2.43	96.9
Grade 1500(*)		2250	2.46	98.2
Sedimented	20.6	2100	2.20	87.9
Sedimented		2150	2.36	94.4
Sedimented		2150	2.39	95.5
Sedimented		2200	2.48	99.1
Sedimented		2250	2.47	98.6

aid. Therefore the addition of some resin-derived carbon improved sinterability in this powder.

An experiment employing a matrix of composition and firing temperature was conducted to identify the optimum carbon content for densification. The ESK Grade 1500 B_4C with the resin-solution addition was used as the test material. All compositions were processed identically and subjected to the heptane wet-milling step (for 10 h) to provide homogeneous

powders. Compacts were die-pressed at 620 MPa and fired by the standard sintering procedure outlined previously. The sintered density results are displayed graphically in Figure 13. The plotted data corresponds to typical values; the densities generally would vary by +/-1% of TD for repeated sintering runs or by +/-2% for different powder batches of the same composition and processing.

The maximum sintered density at each temperature occurred for compositions with 5-6 wt% added carbon. The density values fall off very quickly for lower carbon additions but are not much affected by larger additions. In fact, at the higher firing temperatures the density tends to level off for compositions with 4 to 12 wt% added carbon. The attrition-milled Norton and Aremco powders also sintered well with total excess carbon of $\leqslant$ 6 wt%. These

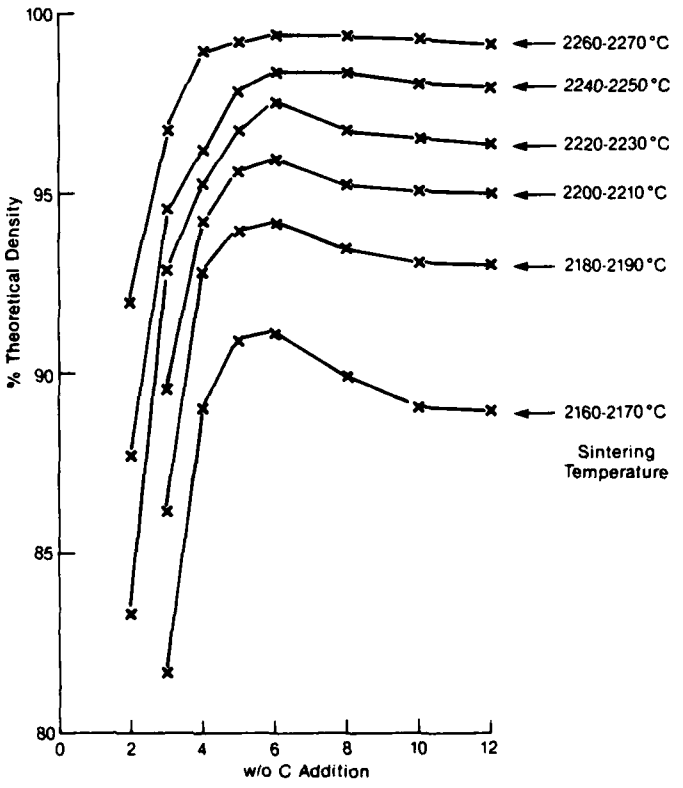

Figure 13 **Sintered density (% of theoretical) vs. wt% C addition for B_4C sintered at various temperatures for 30 min in argon**

latter materials yielded best densities of 96% TD. Sintered density results for these powders and the attrition-milled ESK Grade 1500 are listed in Table 11.

Post-sintering analysis of these compositions showed that graphite was present as a second phase at a level corresponding to the particular amount of carbon addition and that the content of the major impurities (Ti and Si) was unchanged by the firing process. The lattice parameters (by XRD) of the sintered B_4C were slightly decreased relative to the starting powder, indicating that a small amount of carbon had been dissolved.[3] Analysis for total boron and carbon of fired compacts of B_4C with and without added carbon revealed that the solubility was less than 1 wt% carbon and that most of the added carbon was in the form of second-phase graphite. More of the carbon may be in solution at the sintering temperature, but after cooling the composition is near B_4C.

5. Firing temperature

In Figure 13, it can be seen that at the 5-6 wt% carbon addition level, sintered densities are $\geqslant$ 97% TD when sintered at 2220-2230 °C. Higher temperatures add 1 to 2% more density. When fired at 2000 °C, these compositions show little densification so that sintering occurs almost completely above 2000 °C, achieving a density above 90% at 2160-2170 °C. The sintering temperature for B_4C is about 100 to 200 °C above that needed to hot-press B_4C dense[13,14] and roughly 150 °C higher than the sintering temperature for boron-doped SiC.[11]

Of particular interest are the 2 and 3 wt% carbon compositions, which show remarkable gains in sintered density when the sintering temperature is increased from 2160-2170 °C to 2260-2270 °C. Obviously these compositions are sinterable, but only at the highest temperatures. The reason for this is related to the microstructure development in these compositions during sintering and will be treated in the "Microstructure Development in Sintered B_4C" section.

Table 11

SINTERED DENSITIES FOR ATTRITION-MILLED POWDERS

Powder	wt% C Addition	Sintering Temperature (°C)	Sintered Density (g/cm^2)	%TD
Norton*	0	2150	2.11	84.1
	3.5	2150	2.28	91.5
	10	2150	2.21	89.2
	3.5	2200	2.39	95.6
	10	2200	2.32	93.5
	0	2250	2.32	92.7
	3.5	2250	2.38	95.5
	10	2250	2.36	95.2
Aremco*	0	2250	1.93	76.6
	6	2100	2.28	91.1
	6	2150	2.35	93.9
	6	2200	2.40	95.7
	6	2250	2.39	95.4
ESK	0	2250	1.81	71.7
	6	2100	2.34	93.4
	6	2150	2.45	97.8
	6	2200	2.47	98.7
	6	2250	2.47	98.7

*The Norton B_4C contained 5.2 wt% C prior to the listed carbon additions; the Aremco B_4C had 0.9 wt% C V2.0

6. Impurities

The common impurities in the B_4C powders are listed in Table 2. Since these impurities could not be completely removed, an attempt was made to determine their effect on the sintering process. The attrition-milled Norton and Aremco powders contained some free carbon and its effect has been characterized. Oxygen, a major impurity that plays an important role in the sintering process, was discussed earlier. The metallic impurities were of some concern as earlier investigations[15,16,17] claimed some of these (Fe, Ti, Si and Al) to be sintering aids for B_4C. In this study, attempts were made to sinter B_4C with additions of 1 wt% of Fe, Si, Ti, Al as well as elemental boron, but none of these promoted significant densification.

To determine the impurity effects on carbon-doped B_4C a set of compositions were prepared, comprised of a base composition of B_4C + 6 wt% carbon and one of each of the following additives: 1 wt% Si, 1/2 and 1 wt% Al, 2 wt% Ti, and 1 wt% Fe_2O_3). Pressed compacts of each composition were fired at 2160 and 2200 °C. Sintered density results are given in Table 12. At 2200 °C, the impurities do not increase the density, but at 2160 °C Si and Al do enhance the sintered density by 1 to 2%.

Parallel sintering experiments with powder mixtures of B_4C and SiC also showed that Si enhances the sinterability of B_4C. A composition of 70 wt% B_4C and 30 wt% SiC sintered to 90% TD at 2225 °C with no carbon addition while the same composition with 3 wt% added carbon went to 99% TD at 2200 °C. B_4C + 6 wt% carbon with SiC additions of 5 to 30 wt% SiC typically sintered to 95% TD at 2150 °C. Adding Si as SiO_2 had similar effects on the sinterability, but was less satisfactory as the SiO_2 and carbon would react and generate CO gas, which would produce large pores in the sintered material.

The mechanism by which Si (or Al) enhances sintering in B_4C is unknown but may be related either to the formation of a liquid phase or to lattice defects (as the impurities dissolve

Table 12

IMPURITY EFFECTS ON SINTERED DENSITY

Base Composition: B_4C + 6 wt% C

Sintered in argon for 30 min

Additive	Sintering Temperature (°C)	Sintered Density (g/cm^3)	%TD
none	2160	2.35	93.8
1/2 wt% Al	2160	2.39	95.5
1 wt% Al	2160	2.37	94.8
1 wt% Si	2160	2.40	95.8
2 wt% Ti	2160	2.29	91.5
none	2200	2.43	96.9
1 wt% Al	2200	2.37	94.8
1 wt% Si	2200	2.41	96.4
1 wt% Fe	2200	2.41	96.4
2 wt% Ti	2200	2.40	95.8

in the B_4C), the presence of which promotes the diffusion kinetics applicable to densification. Certainly the levels of these impurities in the starting powders is insufficient to provide any significant densification in B_4C without carbon additions.

F. Microstructure Development in Sintered B_4C

The microstructure development of sintered carbon-doped B_4C was sensitive to several factors: sintering temperature, time at temperature, wt% carbon addition and its distribution, and impurity content. Selected sintered compacts were diamond polished and then electrolyti-

cally etched with an aqueous solution of KOH − $K_3Fe(CN)_6$ (Murakami's reagent) to reveal the microstructure.

For the optimum composition of B_4C (ESK Grade 1500) + 6 wt% C, a microstructure composed of fine, equiaxed grains ranging in size from 1-5 μm is obtained upon firing at 2220-2230 °C to 97% TD (Figure 14). Abnormal grain growth begins for this composition during sintering above 2235 °C by the formation of individual or clustered grains of 10 to 30 μm size (Figure 15). At $\geqslant$ 2250 °C, the structure coarsens considerably and develops large grains which exhibit extensive growth twinning (Figure 16). Depending on the exposure, remnant patches of fine grains may be occasionally observed in this coarse-grained microstructure.

As shown in the previous section, increased densification may be realized by sintering at the higher temperatures. However, the attending grain growth is highly detrimental to fracture strength.[f] Additionally, for grain sizes $\approx$ 100 μm transgranular microcracking is evident (Figure 17), a condition that may also contribute to reduced strength. The microcracking is not an unexpected phenomenon since the thermal expansion of the B_4C crystal is anisotropic, a situation that contributes to microcracking in other ceramic systems.[18,19] To determine the degree of anisotropy the change in the hexagonal lattice parameters (a_o, c_o) of B_4C were measured as a function of temperature up to 600 °C. The resulting thermal expansion coefficients are (per °C):

$$a_o = 5.29 \times 10^{-6}$$

$$c_o = 6.25 \times 10^{-6}$$

The expansion anisotropy arises from the difference between the expansions in the directions of the lattice parameters. It is sufficient to induce stresses between B_4C grains and consequently microcracking on cooling from the sintering temperature (see Appendix II).

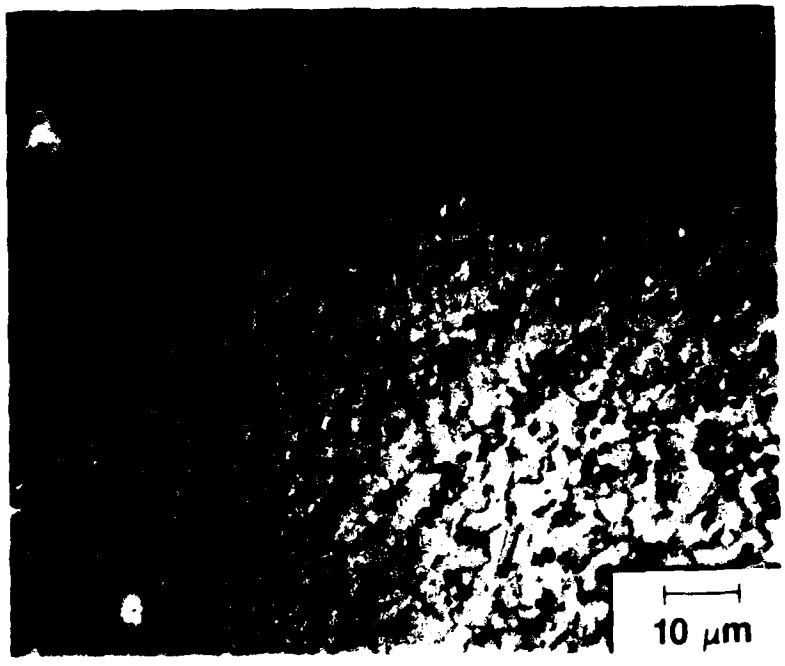

Figure 14. **Polished and etched section of B_4C + 6 wt% C sintered at 2220 °C for 30 min in argon**

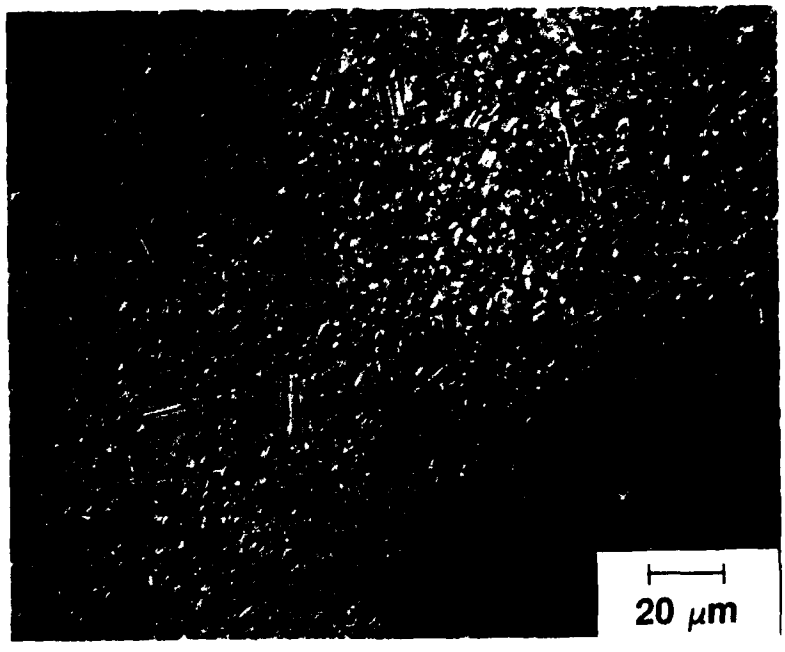

Figure 15. **Polished and etched section of B_4C + 6 wt% C sintered at 2240 °C for 30 min in argon**

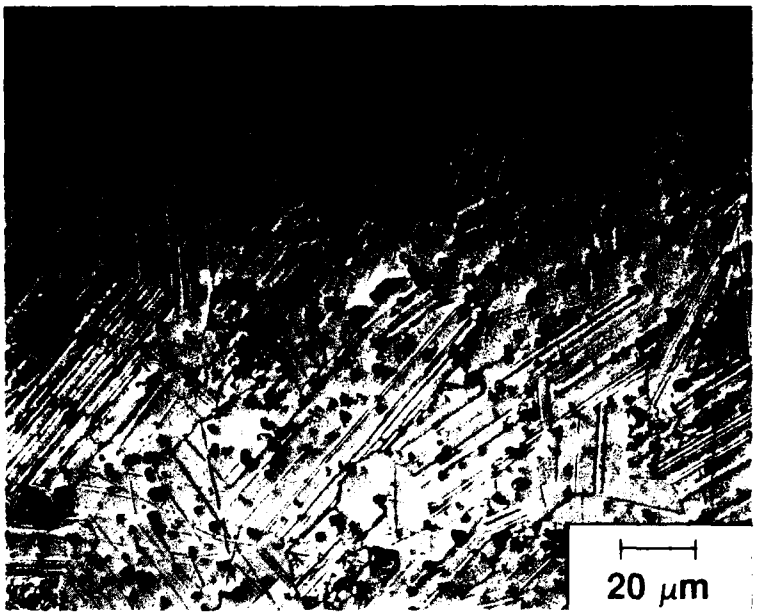

Figure 16. Polished and etched section of B_4C + 6 wt% C sintered at 2260 °C for 30 min in argon

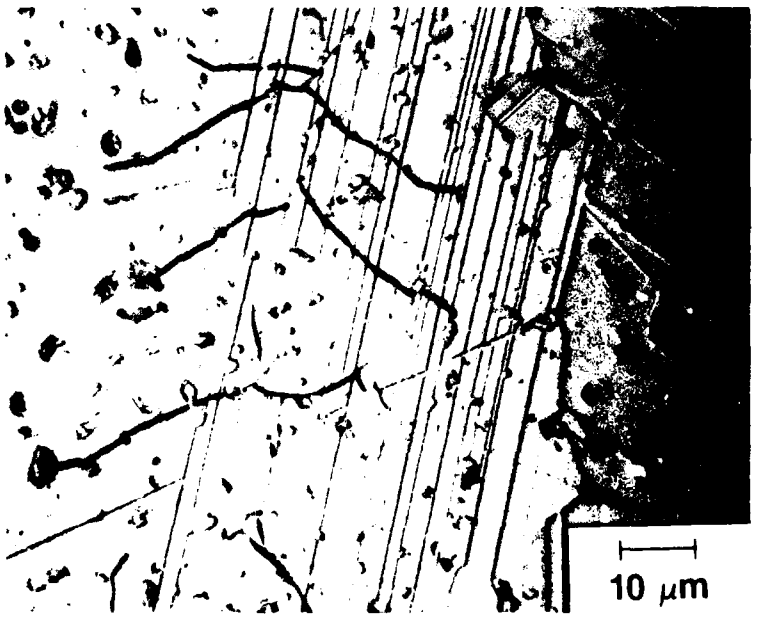

Figure 17. Transgranular microcracking in coarse-grained B_4C

The microstructure development in the composition B_4C + 2 wt% C reveals an interesting relationship between densification and grain growth. When sintered at temperatures below 2200 °C, this composition densifies to no more than 80% TD and the grain size is no more than 5 μm. As the sintering temperature is increased to above 2200 °C, significant grain growth occurs and the density increases, reaching 92% at 2260-2270 °C. Figures 18 and 19 illustrate this change in microstructure. The indication is that grain growth may make a major contribution to densification in compositions that are only marginally sinterable. This density increase is possibly related to the pore stability criterion discussed earlier. In compositions with low carbon addition, the pores may grow to some extent and become stable. When significant grain growth occurs at the higher temperatures, the grain size to pore size ratio increases and the pores become unstable and shrink, thus providing further densification.

The carbon added to B_4C appeared as graphite particles in the sintered microstructure. Generally these were not visible in polished sections since the polishing process tends to remove them; however, with careful slow lapping, the graphite could be revealed. Figures 20 and 21 show the graphite in the microstructure of fine- and coarse-grained structures, respectively. The graphite particles appear as the bright phase with light microscopy using crossed polarizers. The presence of graphite was also identified by XRD.

An interesting feature of the two micrographs is that the nature of the graphite particles changes with the grain size of the B_4C. In the fine-grained structure the graphite particles are intergranular and about 1 μm in size while in the coarse-grained structure the intergranular particles are larger ($\approx$ 5 μm) and many fine particles have been engulfed by the large B_4C grains. The titanium impurity (as TiB_2) also can be found as an intergranular phase in the sintered microstructure as 1 μm particles, but like the graphite, it grows as the B_4C grains coarsen. This growth of second-phase particles probably occurs by coalescence of the small particles as the amount of grain boundary area decreases with increasing B_4C grain size.

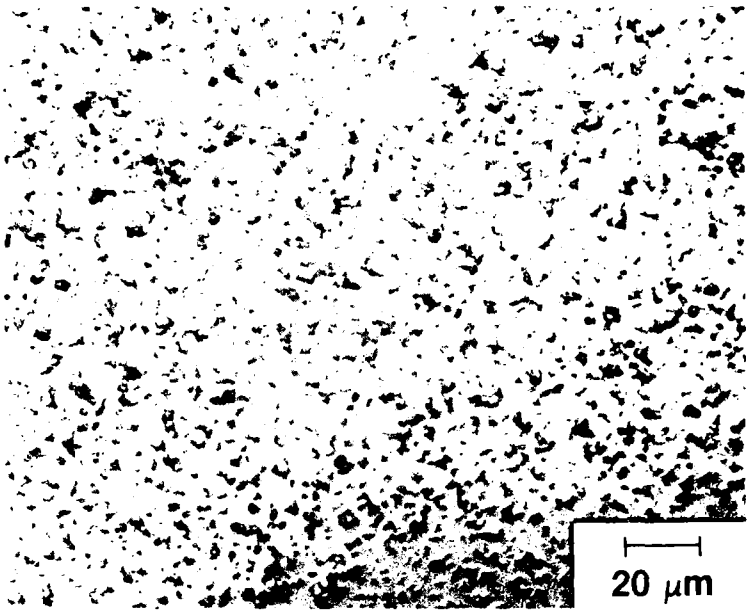

Figure 18. **Polished section of B_4C + 2 wt% C sintered at 2200-2210 °C for 30 min in argon**

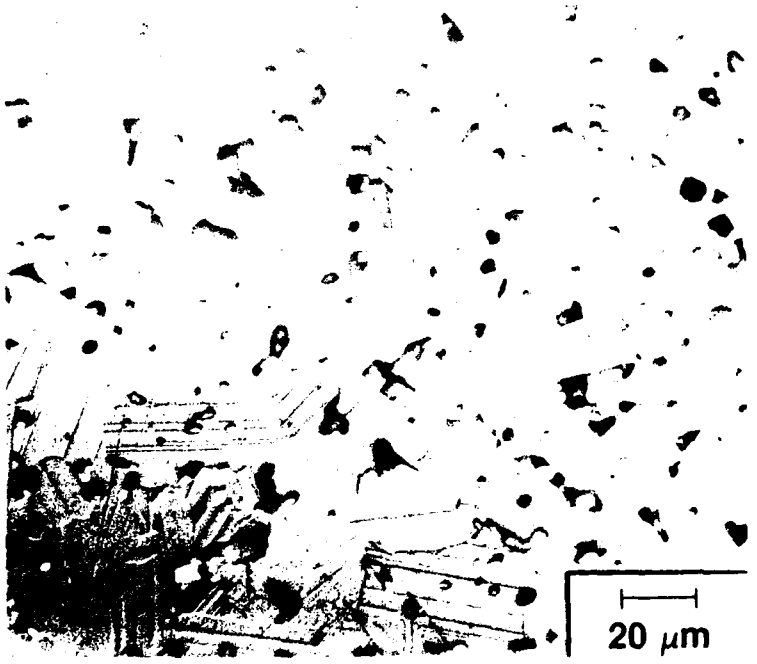

Figure 19. **Polished and etched section of B_4C + 2 wt% C sintered at 2260-2270 °C for 30 minutes in argon**

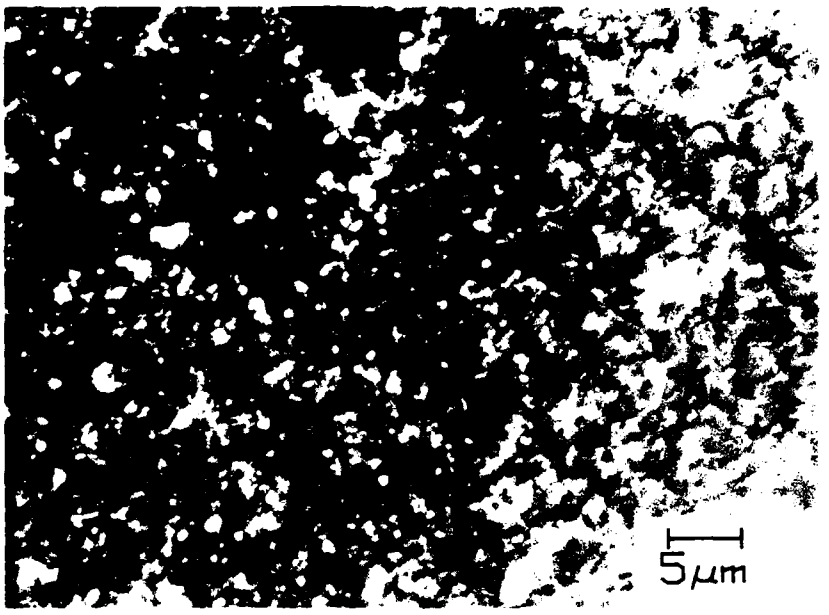

Figure 20. Graphite particles (bright phase) in a fine-grained sintered B_4C microstructure. Revealed with cross-polarized light microscopy.

Figure 21. Graphite particles (bright phase) in a coarse-grained sintered B_4C microstructure. Revealed with cross-polarized light microscopy.

The uniformity of distribution of the added carbon was a major factor in microstructure development. Powder compositions with resin-solution carbon additions that contained agglomerates caused by segregation of the resin often yielded nonuniform sintered microstructures. Figure 22 exhibits this characteristic in a B_4C + 6 wt% C compact sintered at 2250 °C. The agglomerate appears as the elongated fine-grained region which is partially bounded by a crack-like opening. The surrounding microstructure consists primarily of large grains. It was not uncommon to find a large number of these regions in the microstructure. In fine-grained structures these agglomerates appeared as rounded areas of high porosity. The porosity was actually holes left when the polishing process removed the high concentration of graphite particles in the agglomerate region. The size of the agglomerates corresponded to the mesh size through which the processed powder had been screened. Thus, finer mesh screening eliminated some agglomerates and left finer ones which generally resulted in a more uniformly sintered microstructure. The wet-milling process (milling in heptane for 10 to 18 h) successfully removed the agglomerates for compositions with 6 wt% or less added carbon, allowing development of uniform microstructures. For compositions with more than 6 wt% added carbon, some agglomerates generally remained in spite of the wet milling.

An interesting feature of the carbon-segregated agglomerates was that a fine-grained structure could survive in these regions while the surrounding microstructure was undergoing considerable grain growth. This indicated that increased carbon concentration might inhibit the abnormal grain growth. Further evidence for this was gained by the observation of a pronounced surface effect on grain growth. In Figure 23 a B_4C + 6 wt% C specimen fired at 2250 °C is shown, which has a coarse-grained grained structure internally, but from the surface to 200 μm deep the structure is fine-grained. It is believed that this is caused by the removal of boron in the vicinity of the specimen surface during firing by oxygen present in the furnace atmosphere and in the B_4C itself. Consequently, the surface region is depleted in

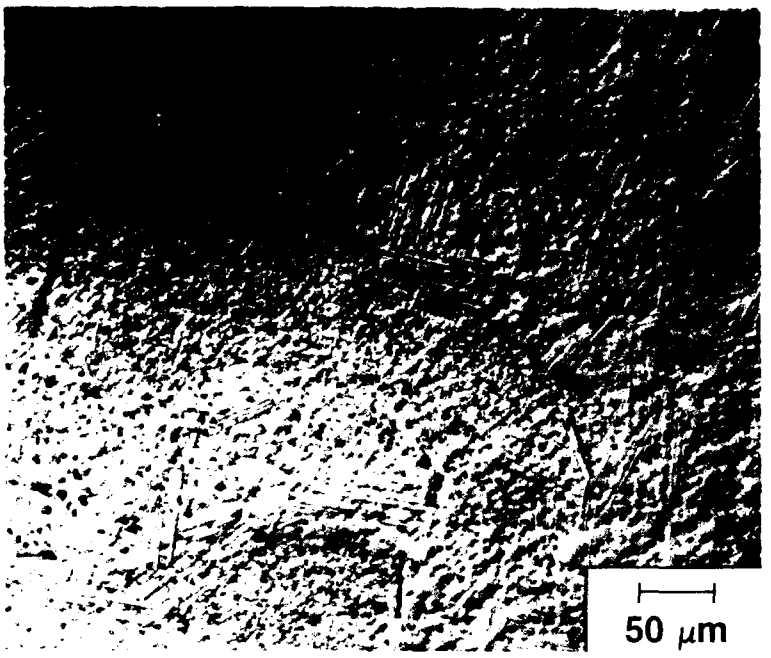

Figure 22. Processing defect (carbon segregation) in a sintered B_4C microstructure. Defect is fine-grained while surrounding structure is coarse-grained.

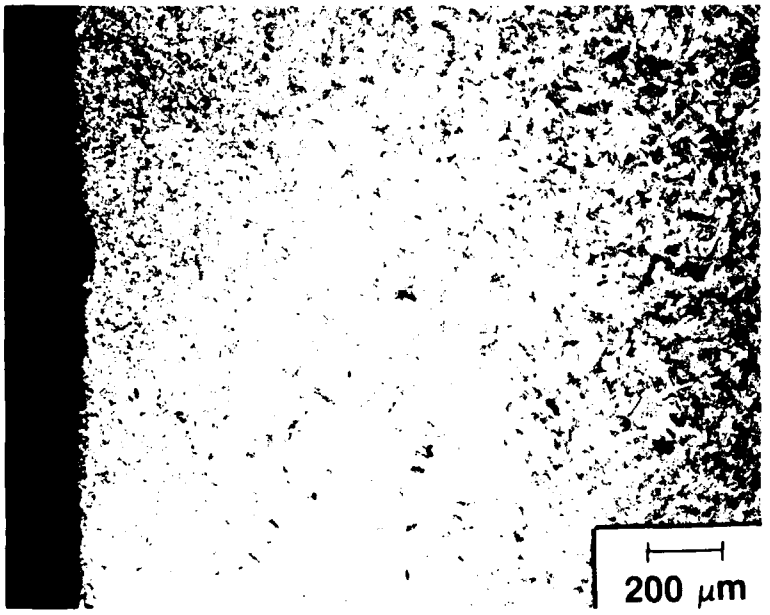

Figure 23. Surface effect in a coarse-grained sintered B_4C microstructure

boron and enriched in carbon, which inhibits the grain growth. At sintering temperatures above 2250 °C, grain growth eventually consumes this surface layer.

Following this realization, compositions with 8 to 12 wt% added carbon were investigated, and indeed the additional carbon inhibited grain growth without seriously affecting densification. Compositions with a well-distributed 12 wt% C could be fired at 2270 °C to 99% TD and would give a fine-grained ($\leqslant 10\ \mu m$) microstructure.

Thus, it is apparent that carbon is instrumental in controlling the grain growth process in B_4C. Since the graphite particles tend to be intergranular, the mechanism of grain growth inhibition is expected to be second phase particle drag on grain boundaries. In such a system, excessive grain growth would be abnormal; that is, grains would initially grow in isolated areas where the second-phase particles are deficient. Such a pattern is observed in B_4C. This phenomenon also points out the importance of the uniformity of distribution of the added carbon on the development of uniform microstructure in sintered B_4C.

As a function of time, the normal grain growth process in B_4C is slow. The composition B_4C + 6 wt% C fired at 2000 °C shows little densification and a grain size on the order of 1 μm. When sintered at 2220-2230 °C to 97% TD, the grain size only increases to a maximum of about 5 μm in 30 min at temperature. Extended hold time at temperature produces only small changes in grain size.[1]

When abnormal grain growth occurred, it was not necessarily an extremely rapid process. Compacts of B_4C + 6 wt% C were fired at 2240-2250 °C for 10, 30, or 60 min to determine how quickly large grains may form. At 10 min the density reached 97% TD and the microstructure was composed of fine grains 1 to 5 μm in size. At 30 min the density was 98% and the microstructure contained isolated grains 10 to 15 μm in size in a matrix of 1 to 5 μm grains. After 60 min the density was 99% and grains 20 to 40 μm size comprised about 75%

of the structure with the remaining grains $\leqslant 10\ \mu m$. A compact of B_4C + 12 wt% C subjected to the same 60 min firing was 98% dense with a 1 to 6 μm fine-grained structure.

The onset of the abnormal grain growth, while inhibited by free carbon in the structure, may be induced by the impurities present in the B_4C. It was observed previously that sintered B_4C containing some tungsten carbide milling impurity experienced extreme grain growth due to formation of a liquid phase.[20] This was verified by sintering B_4C with 1 wt% intentionally added tungsten carbide. At this high level of impurity, grains larger than 200 μm were formed, which is twice that normally observed in B_4C without the impurity. Significant tungsten is not present in the B_4C material, but the impurities Si, Fe, Ti, and Al are present at $\geqslant$ 100 ppm levels in some or all of the B_4C powders used, and these may be responsible for promoting the exaggerated grain growth.

The specimens discussed earlier that were sintered at 2200 °C, with additions (1/2 to 2 wt%) of the impurities, were sectioned, polished, and etched to observe the condition of the microstructures, which are shown in Figures 24, 25, 26, and 27. A control specimen with no impurity addition sintered in the same firing showed no abnormal grain growth. It is apparent from the micrographs that Si, Fe and Al generate abnormal grain growth while Ti has no effect. Most likely the grain growth is assisted by a liquid phase formed with the impurity. The state of the Fe or Al is unknown, but the sintering temperature is well above their melting points. Silicon probably reacts with carbon to form SiC and at low concentration may dissolve in B_4C. Compositions of the reported B_4C-SiC eutectic composition (70 wt% B_4C − 30 wt% SiC)[21] were observed to melt at 2240-2250 °C. This eutectic melt temperature corresponds closely to the temperature at which considerable abnormal grain growth occurs in sintered B_4C. However, this may be misleading since the amount of silicon present in the ESK B_4C (700 ppm) may be entirely dissolved in the B_4C and not available to the eutectic composition. The reported solubility of silicon in B_4C is 0.36 wt% at 2100 °C.[22] Nevertheless

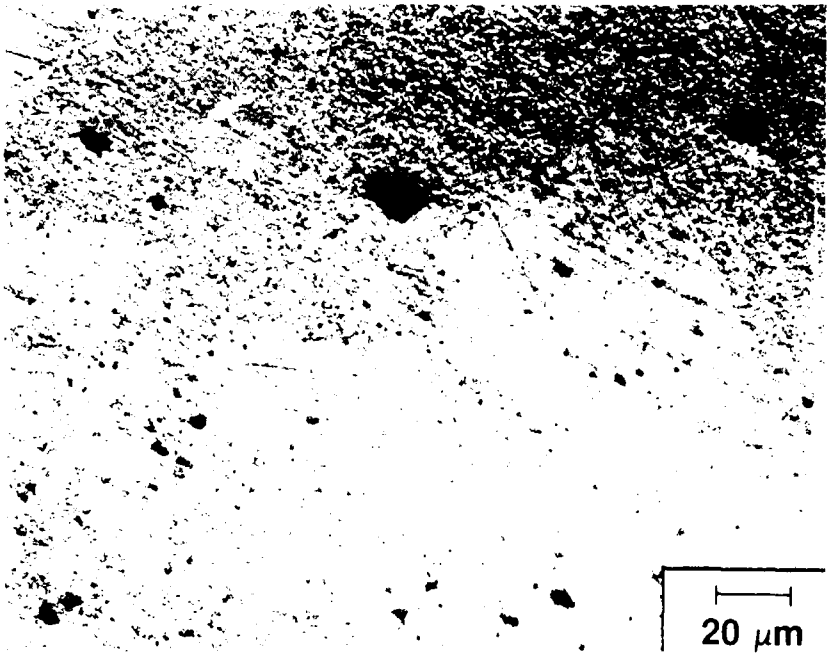

Figure 24. **Polished and etched section of B_4C + 6 wt% C + 1 wt% Si sintered at 2200 °C**

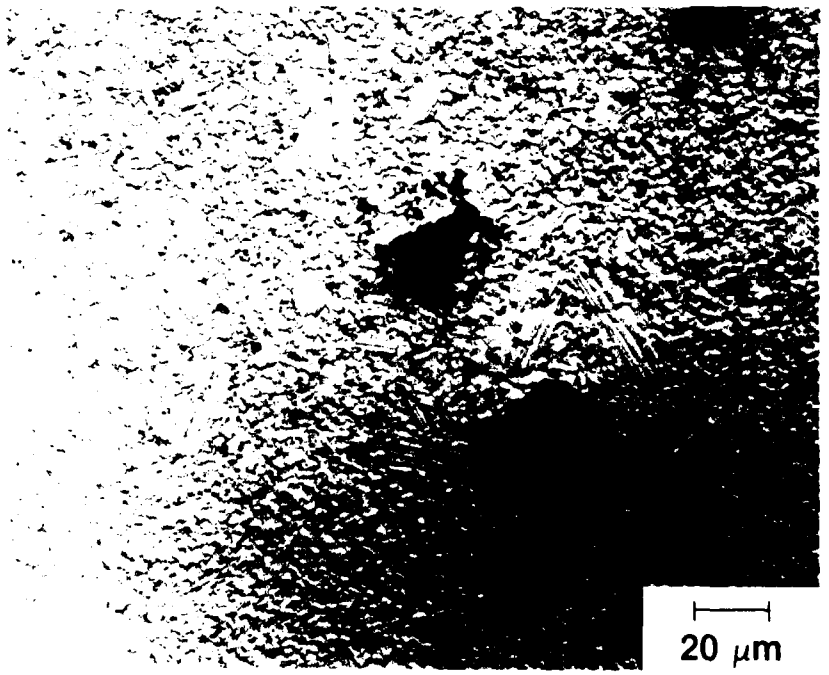

Figure 25. **Polished and etched section of B_4C + 6 wt% C + 1 wt% Fe sintered at 2200 °C**

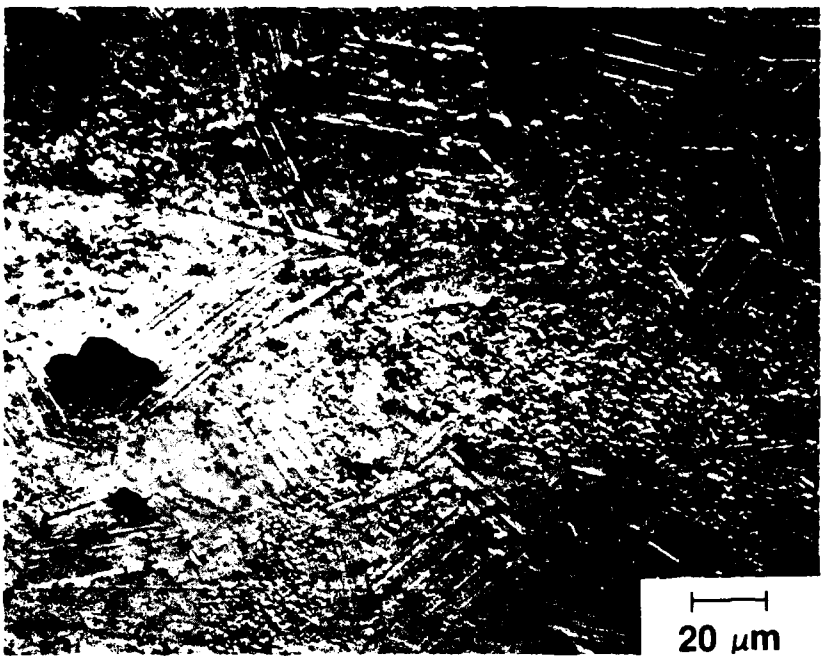

Figure 26. **Polished and etched section of B_4C + 6 wt% C + 1 wt% Al sintered at 2200 °C**

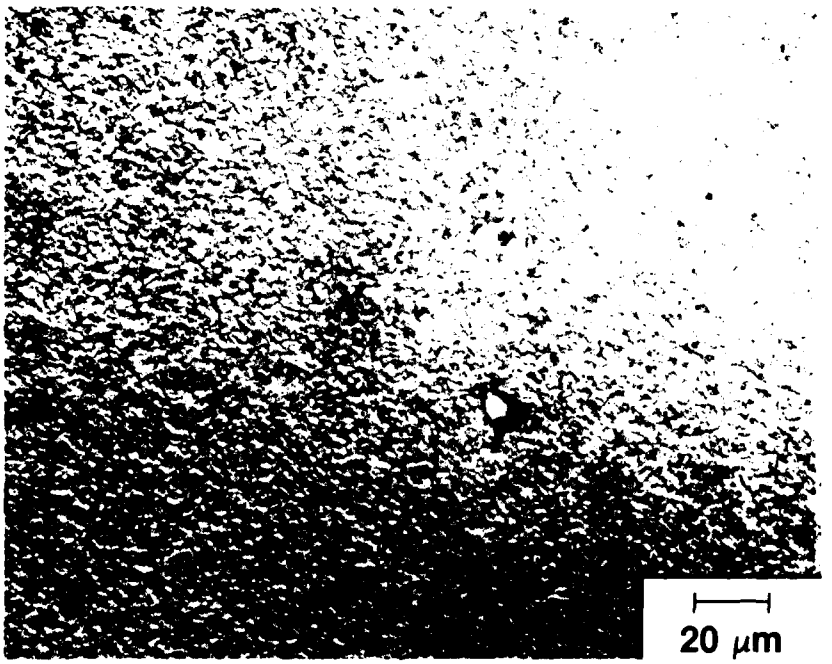

Figure 27. **Polished and etched section of B_4C + 6 wt% C + 2 wt% Ti sintered at 2200 °C**

at a high level (1 wt%) the silicon content may be sufficient to produce a liquid phase. The effect of Fe and Al on grain growth follows similar reasoning. The lack of effect by Ti results from its tendency to form the refractory compound TiB_2, which, like the graphite particles, resides in the structure as an intergranular phase.

Evidence of a second phase (possibly the source of a liquid at elevated temperatures) was found in TEM sections where small, generally submicron particles were observed on B_4C grain boundaries. X-ray spectroscopy was used to determine the elemental constituents of the particles. Many of these particles were the TiB_2 second phase, but some of them contained Si and Fe. Thus, some of the silicon and iron are at least in the form of a second phase which may be the source of a liquid phase at the sintering temperature inducing grain growth.

The likelihood of a B_4C-C eutectic liquid alone causing the abnormal grain growth is doubtful since specimens with 12 wt% added carbon (beyond the solubility limit of carbon in B_4C)[23] showed no abnormal grain growth at 2270 °C and no evidence of melting when heated to 2300 °C. The eutectic temperature is apparently at a much higher temperature than those employed in this study. However, these components could be part of a liquid formed with the impurities in the system.

III. MECHANICAL PROPERTIES OF BORON CARBIDE AND STRUCTURES

A. Summary of Previous Work

During the initial year's effort significant results related to mechanical properties of boron carbide and structures were:[1]

1. Internal friction (inherent material damping capacity) was determined for B_4C and several other representative materials by measuring the free decay of vibrating free-beam specimens. Boron carbide was found to possess an internal friction value considerably higher than such materials as steel, aluminum, and aluminum oxide ceramic.

2. The internal friction of B_4C was independent of frequency in the range of 500 to 8000 Hz.

3. The effect of porosity on the internal friction was minimal, increasing by a factor of 2 for a decrease in density from > 95% to 58% TD. The corresponding elastic modulus was decreased by $\approx$ 6 times.

4. Measurements on high aspect ratio specimens in a cantilevered beam configuration showed that the mechanical damping capacity was strongly influenced by the clamping apparatus. Enough of the mechanical energy of the vibrating beam escaped through the clamp so that the damping capacity of a B_4C beam was increased by 34 times at a frequency of 88 Hz and by 4 times at 558 Hz.

5. A simple and highly effective way to enhance the damping capacity of a cantilevered beam using a rubber insert in the clamping assembly was evaluated and found to increase the damping capacity of the test beam by 100 times.

6. The tensile elastic modulus of 98% dense B_4C was found to be > 400 GPa.

7. Fracture strength was measured in three-point bend for a number of hot-pressed and sin-

tered B_4C specimens. The development of a coarse-grained microstructure was found to be detrimental to the fracture strength.

B. Damping Capacity and Elastic Modulus

The inherent damping capacity or internal friction of B_4C was determined by vibrating a free-beam specimen at its fundamental flexural resonant frequency and then observing the free decay of the vibration. The elastic modulus could be calculated from the value of the resonant frequency. Details of this procedure were given in an earlier report.[1]

The objective was to evaluate these properties for B_4C (and ultimately for structures formed with B_4C elements) relative to other representative materials and subsequently to develop a means to enhance the damping capacity without seriously affecting other properties. The damping capacity of B_4C was generally higher than that for typical ceramics and metals; however, the material is by no means a highly damped material such as rubber. So it was necessary to look for ways to increase the damping capacity of B_4C.

Dense B_4C possesses a high elastic modulus (stiffness) and, when coupled with a low specific gravity (2.52 g/cm^3), one of the highest stiffness to weight ratios of all materials. Given a reasonable strength, it qualifies as a potentially good structural material, particularly for spacecraft applications where mass is a prime consideration. To maintain these properties, significant changes in B_4C to effect increased damping capacity are limited. A few ways have been attempted but without much positive effect. Increased porosity doubles the internal friction but at the expense of a greatly decreased elastic modulus. Sintered B_4C with either a coarse-grained structure (grain size = 50 to 100 μm) or large carbon additions (12 wt% C) has virtually the same internal friction as the standard, dense, fine-grained B_4C despite the presence of microcracks in the coarse-grained material or the large amount of free graphite (which has a higher damping capacity than B_4C) in the high carbon content material. How-

ever, both of these variations lead to decreased strength. It is interesting that the microcracking in the coarse-grained material has no noticeable effect on the internal friction or the elastic modulus in contrast to other microcracked ceramic materials which exhibit significant changes in these properties.[18,19] It is possible that microcracking in B_4C is not as severe as it is in other systems. The addition of silicon carbide, a suitable alloying agent, to B_4C also affects the damping capacity very little. The damping and modulus measurements are summarized in Table 13.

The conclusion that may be maae is that changing the damping capacity of B_4C by materials design techniques is not a very promising approach. Alternatively, enhanced damping capacity should be approached through structural design and indeed this proves to be a simpler and more effective means. There are certainly many ways to do this, but the method chosen should be a simple one that introduces a minimum of volume and mass to the structure and that maintains the integrity of the structural assembly. The second of these requirements is

Table 13

EFFECT OF MICROSTRUCTURAL AND COMPOSITIONAL CHANGES ON INTERNAL FRICTION AND ELASTIC MODULUS OF BORON CARBIDE

Composition	Microstructure	%TD	Internal Friction	Elastic Modulus (GPa)
B_4C + 6 wt% C	fine-grained	98	6.5 × 10–4	404
B_4C + 6 wt% C	coarse-grained and microcracked	96	6.2 × 10–4	388
B_4C + 12 wt% C	fine-grained	93	6.1 × 10–4	309
B_4C	fine-grained and porous	58	10 × 10–4	62
70/30 wt% B_4C/SiC + 3 wt% C	fine-grained	97	3 × 10–4	379

based on the need for a potential spacecraft structure. To evaluate structural design effects, it was necessary to run tests on a realistic structure such as a cantilevered beam.

An important characteristic of a structure comprised of a high aspect ratio beam attached at one end to a rigid base is that when the beam vibrates, much of the vibrational energy may be lost through the base. Physically this process is quite simple. When the free end of the cantilevered beam is deflected and caused to vibrate by some force, a roughly equal force is applied to the fixed end of the beam. Since the fixed end is not free to vibrate, elastic strain results. If the beam material has a high stiffness, much of the force will be applied to the rigid base, which will in turn be strained as well. In this way the vibrational energy is transmitted from the beam into the base. Since mechanical damping is accommodated by the loss of vibrational energy, this provides an enhanced damping to the beam. This characteristic is particularly true if the beam material is of the same or greater stiffness than the base material, as will be the case with a B_4C beam.

The cantilevered beam test apparatus was described previously.[1] With this rig, it was observed that beams of B_4C and stainless steel exhibited higher damping capacity than warranted by previously measured internal friction values. This increase was due to vibrational energy losses through the clamp assembly. Damping capacity was further enhanced by adding a rubber damping element at the clamping point. The damping element was able, owing to its inherently high damping capacity, to dissipate much of the vibrational energy. Figure 28 illustrates the test apparatus with the damping element. Again the damping is measured by observing the free decay of vibrations in the beam.

Because of the effectiveness of the damping element, further investigation of this configuration followed. For ease of fabrication, 304 stainless steel was chosen as the beam material. Operating at low vibrational deflection levels assured that the beam was bending in

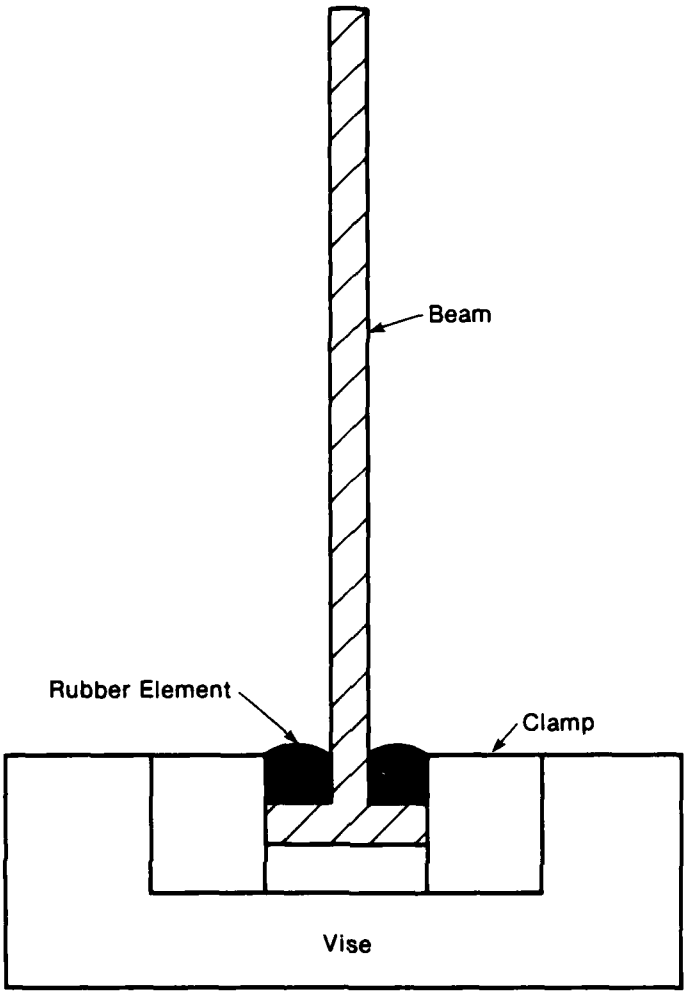

Figure 28. Cantilevered beam with rubber damping element

an elastic mode so that its response would be characteristic of other elastic materials such as B_4C. The beam was 7.25 in. long by 0.375 in. wide and 0.05 in. thick. One end of the beam had a section 0.25 in. high by 0.25 in. thick that was clamped in the test rig between tungsten carbide grips. Damping tests were carried out using three different configurations: 1) with no damping element in the assembly, 2) with a damping element between the beam base and the tungsten carbide grips, and 3) with a damping element in the clamp but only partially between the grips and the beam (as in Figure 28). Two damping elements 0.5 in. square by 0.125 in. thick were used – one for each clamped face of the beam. These were squeezed

into place by tightening the grips onto the beam with the damping elements in position. Damping element material was either rubber, lead (Pb), or textilite (bonded cellulose). Damping capacity results are shown in Table 14.

Clearly the damping capacity of the cantilevered steel beam is much higher than the internal friction of this material (1.5×10^{-4}) measured in the free-beam mode. In configuration #2 with the damping element in the base, little is changed using lead or textilite. This is probably because the damping element has little opportunity to deform and dissipate vibrational energy when tightly clamped between the beam base and the rigid grips. The rubber element provides some increased damping since it is able to deform even within the rigid clamp. This configuration for the damping element does not appear very promising and may be detrimental to structural integrity as the element forms a physical link between the clamp and beam.

Table 14

DAMPING CAPACITY OF 304 STAINLESS STEEL CANTILEVERED BEAM WITH DAMPING ELEMENT

Configuration(#)	Resonant Frequency (Hz)	Damping Capacity
No damping element (1)	33.1	4.1×10^{-3}
Textilite in base (2)	33.1	4.5×10^{-3}
Lead in base (2)	33.1	4.2×10^{-3}
Rubber in base (2)	32.9	7.9×10^{-3}
Lead near base (3)	39.5	9.7×10^{-3}
Rubber near base (3)	35.3	27.5×10^{-3}

The best enhancement of damping capacity is achieved with the damping element around the base in configuration #3. In this mode structural integrity is retained because the grips clamp directly onto the beam. The damping element contacts the beam at a point where the beam is not otherwise rigidly constrained and so some beam deflection is present. Thus the damping element experiences more deformation and dissipates vibrational energy to a greater extent. The rubber element was the most successful in promoting damping as might be expected from its naturally high internal friction value (0.2). Thus an extremely high damping capacity (only an order of magnitude less than rubber itself) can be imparted to a cantilevered beam using a low-volume, low-mass damping element. While rubber may not be suitable for use in space, a usable and comparably high damping material can most likely be identified.

C. Fracture Strength of Boron Carbide

The strength of a high-stiffness ceramic material in a structural application is an important property because only relatively small deflections can occur in a beam of such a material before brittle fracture occurs. Unlike metals, no plastic deformation takes place to offset applied stresses in a ceramic such as B_4C.

Three-point bend testing was applied to B_4C test bars (1.25 in. × 0.125 in. × 0.125 in.) using an Instron testing machine with a 1 in. span and a crosshead speed of 0.02 in. per min. All test specimens were machined longitudinally to avoid alignment of machining flaws perpendicular to the applied stress except in one set of hot-pressed specimens where cross-cut machining was intentionally used to study the effect of machining flaws. The effects of compositional, microstructural, and processing variations on the flexural strength were evaluated.

Table 15 lists the flexural strength data accumulated for B_4C in this study. Each data point represents an average for 6 to 10 test specimens. Ranges are shown for the strength values where several sets of test bars have been prepared and tested. In all cases, fracture was

Table 15

FLEXURAL STRENGTH OF BORON CARBIDE

Material	Microstructure	%TD	Fracture Strength (MPa)
Hot-pressed B_4C longitudinally machined	fine-grained	94-95	490
Hot-pressed B_4C cross-cut machined	fine-grained	94-95	414
B_4C + 6 wt% C no wet milling	fine-grained	93-97	140-400
B_4C + 6 wt% C wet milled	fine-grained	98	557
70/30 wt% B_4C/SiC + 3 wt% C wet milled	fine-grained	99	575
B_4C + 12 wt% C wet milled	fine-grained	95-96	290
B_4C + 6 wt% C some wet milled	coarse-grained	94-97	160-230
B_4C	fine-grained and porous	58	219

transgranular as exemplified by a typical fracture surface shown in Figure 29. Strength of hot-pressed B_4C is comparable to that measured by others[2,13] and provides a baseline for comparison to strengths of pressureless sintered B_4C since the hot-pressed material's strength is reasonably high for a monolithic ceramic. Some sensitivity to machining flaws is evidenced by the 15% decrease in strength for test bars machined cross-wise so that machining flaws were perpendicular to the applied stress.

Some of the sintered carbon-doped B_4C exhibited strengths of 400 MPa, but the strength was inconsistent for different sets of test bars. Very low strengths (< 200 MPa) were often

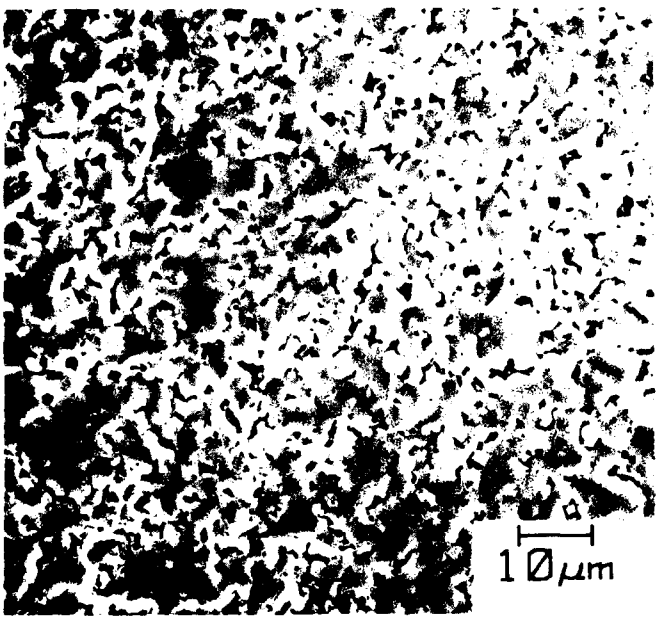

Figure 29. SEM micrograph of fracture surface of strength test bar (composition: B_4C + 6 wt% C).

the case. When the wet milling process (described earlier in this report) was utilized in powder preparation, the strength increased dramatically to a value (557 MPa) higher than that for the hot-pressed material. This was also true for a wet-milled composition of 70/30 wt% B_4C/SiC with 3 wt% added carbon. The typically low strength of material with no wet milling resulted from flaws associated with high carbon concentrations generated by the segregation of the resin additive in the processed powder. Figure 30 shows the fracture surface of such a low-strength material. The uneven, rough surface is the result of the carbon segregations distributed throughout the material. When the segregations are removed by wet milling, a smoother, ridged fracture surface appears (Figure 31) and higher strength is attained. Fracture origins in the high-strength material were typically near the tensile surface and often contained small lumps (or holes), indicating that some small carbon segregations remain and act as critical flaws. Thus, further improvements in processing should increase the fracture strength to yet higher values as these flaws are removed.

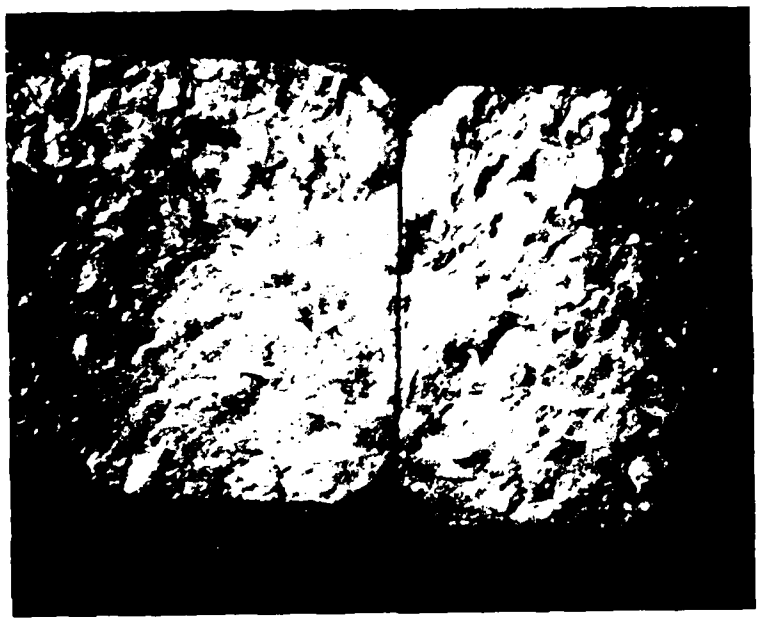

Figure 30. Typical fracture surface of low strength B_4C test ban containing many regions with carbon segregation. Both halves of fractured bar are shown. Width of test bar is 0.125 in.

Figure 31. Typical fracture surface of high-strength B_4C test bar. Both halves of fractured bar are shown. Width of test bar is 0.125 in.

Increasing the carbon concentration enhanced the likelihood of carbon segregations, and with 12 wt% added carbon even the wet milling process was relatively ineffective. Fracture surfaces for sintered B_4C + 12 wt% C were rough (as in Figure 30), and the strengths were fairly low (290 MPa).

Sintered B_4C with a coarse-grained microstructure (grain size $\geqslant$ 50 μm) yielded low strengths as well. The presence of large graphite particles and pores which grow with the B_4C grains may provide the strength-limiting flaws. Alternatively, the strength may be lower because the fracture is transgranular and encounters fewer grain boundaries in the coarse-grained material. Thus the crack moves easily across the large grains and is less often deflected by encounters with grain boundaries. With very large grain size ($\approx$ 100 μm), the observed transgranular microcracking may also contribute to ease of fracture. In fact, even where microcracks have not formed in the coarse-grained material, the residual stresses imposed by the thermal expansion anisotropy are still present and can aid the fracture process.

Porous material (58% TD) naturally has low strength because there is less bonding between grains to resist fracture. It is interesting, however, that the porous material was stronger than some of the dense B_4C that possessed carbon segregations or a coarse-grained microstructure. This emphasizes the severe effect these features can have on strength.

With proper processing and microstructure control, quite respectable flexural strength may be obtained for sintered B_4C.

REFERENCES

[1] S. Prochazka and S.L. Dole, "Development of Spacecraft Materials and Structure Fundamentals," Annual Report, May 31, 1984, No. 84SRD033, G.E. Comp. Schenectady, NY.

[2] K. Schwetz and W. Grellner, "The Influence of Carbon on the Microstructure and Mechanical Properties of B_4C," *J. Less-Common Met., 82,* 37-47 (1981).

[3] R.D. Allen, *J. Am. Chem. Soc., 75,* 3582-3 (1953).

[4] M. Bouchacourt and F. Thevenot, "Analytical Investigation in the B-C System," *J. Less-Common Met., 82,* 219-226 (1981).

[5] D.E. Wittmer, "Use of Bureau of Mines Turbomill to Produce High-Purity Ultrafine Nonoxide Ceramic Powders," Report No. 8854, U.S. Bureau of Mines, Tuscalosa Center, Alabama.

[6] T.P. Hezbell, T.K. Glasglow, and N.W. Orth, "Demonstration of a Silicon Nitride Attrition Mill for Production of Fine Pure Si and Si_3N_4 Powders," Ceramic Bull., 63 (9), 1176 V (1984).

[7] J.L. Hoyer and A.V. Petty, "High Purity Fine Ceramic Powders Produced in the Bureaus' Turbomill," Proc. Conf. on Ceramic Raw Materials, University of Alabama, March 1985 (To be published).

[8] P. Greil, Max Planck Institute, Pulvermetalurgisches Laboratorium, Stuttgart.

[9] C.D. Greskovich and J. H. Rosolowski, "Sintering of Covalent Solids," *J. Am. Ceram. Soc., 59* (7-8) 336 (1976).

[10] W.D. Kingery and B. Francois, "The Sintering of Crystalline Oxides, I. Interactions Between Grain Boundaries and Pores," in *Sintering and Related Phenomena,* G.C. Kuc-

zynski, N.A. Hooten and C.F. Gibson, Ed., Gordon and Breach, NY, 1967.

[11] S. Prochazka, "Sintering of Silicon Carbide," General Electric Co., Report No. 73CRD325 (1973).

[12] H. Suzuki and T. Hase, "Some Experimental Consideration on the Mechanism of Pressureless Sintering of Silicon Carbide," in *Factors in Densification and Sintering of Oxide and Non-oxide Ceramics,* S. Somiya and S. Saito, Ed., 1978.

[13] T. Vasilos and S.K. Dutta, "Low Temperature Hot-Pressing of Boron Carbide and its Properties." *Bull. Am. Cer. Soc., 53,* 453 (1974).

[14] R. Angers and M. Beauvy, "Hot-Pressing of Boron Carbide," *Ceramics International,* 10, No. 2, 49-55 (1983).

[15] D. Stibbes and C.G. Brown, "Cold Pressed Compositions," U.S. Pat. 3149571, July 31, 1973.

[16] R.G. Lange and Z.A. Munir, "Sintering of Pure and Doped Boron Carbide," *Mat. Sci. Res., 13,* G.C. Kuczynski, Ed., Plenum Press, NY, 1980.

[17] G.Q. Weaver, "Sintered High Density Boron Carbide," U.S. Pat. 4320204, Mar. 16, 1982.

[18] S.L. Dole, O. Hunter, Jr. and C.J. Wooge, "Elastic Properties of Monoclinic Hafnium Oxide at Room Temperature," *J. Am. Ceram. Soc., 60* (11-12) 488 (1977).

[19] J.A. Kuszyk and R.C. Bradt, "Influence of Grain Size on Effects of Thermal Expansion Anisotropy in $MgTi_2O_5$," *J. Am. Ceram. Soc., 46* (11) 535-40 (1973).

[20] S.L. Dole and S. Prochazka, "Densification and Microstructure Development in Boron Carbide," To be published in *Ceramic Engineering and Proceedings of the 9th Annual Conference on Composites and Advanced Ceramics,* Cocoa Beach, Florida, January, 1985.

[21] D.R. Secrist, "Phase Equilibria in the System Boron Carbide-Silicon Carbide," *J. Am. Ceram. Soc., 47,* (3) 127-130 (1964).

[22] T. Hase and H. Suzuki, "Solubility and Diffusion of Si in B_4C," *J. Am. Ceram. Soc., 64,* C-58 (1981).

[23] M. Beauvy, "Stoichiometric Limits of Carbon-Rich Boron Carbide," *J. Less-Common Met., 90,* 169-175 (1983).

[24] W.F. Hillebrand, G.E.F. Lundell, H.A. Bright, and J.I. Hoffman, *Applied Inorganic Analysis,* Second Edition, John Wiley and Sons, NY (1953).

Appendix I

Analytical Techniques for B_4C Powder Characterization

1. Total carbon: Powder samples were ignited in flowing oxygen and the generated CO_2 measured gravimetrically after absorption by NaOH.

2. Metallic impurities: Powder samples were dissolved in a boiling mixture of two parts H_2SO_4 and 1 part 70% $HClO_4$. Concentrations of dissolved components were then determined by spectrographic analysis.

3. Total boron: Solutions formed as above were treated with mannitol and then titrated with NaOH[24]

4. Free carbon: Uncombined carbon was detected qualitatively by XRD as graphite; determined quantitatively from analysis of total carbon and boron as the variation from the B_4C composition.

5. Particle size: Determined using a light scattering detection system to analyze the particle size distribution of a centrifugally sedimented powder sample in a liquid suspension.

6. Specific surface area: Determined by low-temperature adsorption and desorption of nitrogen (BET method).

7. Oxygen and nitrogen content: Powder samples were fused in inert gas with graphite to release CO_2 and N_2, which were quantitatively analyzed by gas chromatography.

8. Lattice parameters: Determined by conventional X-ray diffraction (XRD).

Appendix II

(Attached paper: "Abnormal Grain Growth and Microcracking in Boron Carbide")

ABNORMAL GRAIN GROWTH AND MICROCRACKING IN BORON CARBIDE

S. Prochazka, C.I. Hejna, and S.L. Dole

Boron carbide ceramic has been traditionally manufactured by hot pressing of B_4C powders of particle size 1 to 5 μm at temperatures of about 2100 °C. Although this has been a routine process, bodies with very low porosity are difficult to obtain. In recent years, several investigations studied the sintering in B_4C[1-5] and demonstrated that polycrystalline bodies with high densities can be obtained by the press-and-sinter approach. This approach will make possible the fabrication of B_4C configurations previously not feasible such as tubes or other hollow shapes. The essence of these developments was the observation that carbon additions beyond the B_4C molar ratio promoted densification and coincident with very fine, submicron starting powders made possible the attainment of high-density materials on sintering of pressed bodies near 2200 °C in argon. The effect of the excess carbon has been attributed to either suppression of grain growth or to the formation of a eutectic melt in the B_4C-C system; however, the mechanism has not been studied in detail and many related problems remain open.

In the present communication, we report on abnormal grain growth and the related microcracking in boron carbide observed during sintering experiments discussed in Reference 6. The study was done with a B_4C powder (Tetrabor 1500, ESK Corp, Tonowanda, NY*) of average particle size of 1.08 μm and a specific surface area of 12 m^2/g to which 3 to 6% by weight of carbon was added in the form of a phenolic resin.† The components were mixed as a slurry in methanol, dried at room temperature, screened through a 40-mesh sieve, and die-pressed to 1-cm diameter pills of about 60% of theoretical density. The sintering was carried out in flowing argon on carbon setters in a carbon resistance furnace at 2200 °C to 2250 °C. The densities of the sintered specimens varied depending on sintering and processing parameters,[6] ranging up to 97% of the theoretical density of B_4C (2.52 g/cc).

The grain structure was revealed by electrolytic etching of polished and lapped sections in a diluted Murakami's reagent. The microstructures showed that the specimens underwent exaggerated grain growth when the sintering temperature exceeded 2220 °C as shown in Figure 1. The large grains grew randomly in a relatively fine grained matrix of equiaxed grains about 2-4 μm in size. The large grains also frequently showed entrapped inclusions and pores in addition to engulfed B_4C grains of different orientation that indicate rapid grain boundary advancement. Indeed, near 2250 °C, the growth occurred in minutes while the matrix grains barely changed in size.

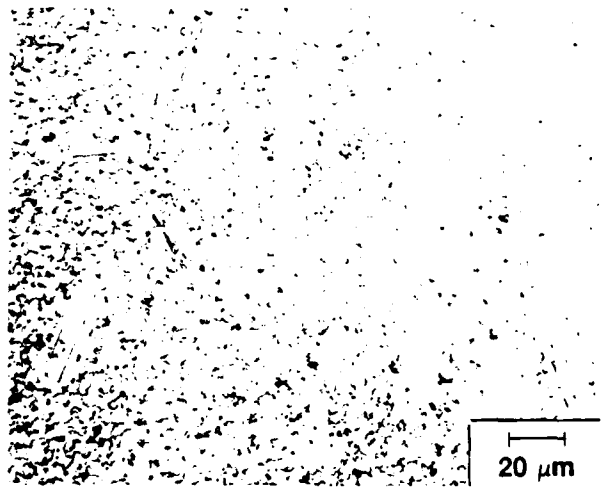

Figure 1. Incipient exaggerated grain growth in sintered boron carbide. Etched specimen; interference contrast.

The new grains give the same diffraction pattern, and consequently, this growth can be classified as abnormal or exaggerated grain growth that has been observed in numerous other ceramic systems. It has been frequently associated with the presence of small amounts of a liquid at the annealing temperature,[7] although examples of exaggerated grain growth proceeding in the absence of a liquid do occur (SiC, MgO). In the present case, microstructural evidence of a liquid has not been obtained except for isolated cases such as shown on Figure 2 where the presence of

* Composition in %: total carbon 21.3, oxygen 1.46, Ca 0.1, Mg 0.01, Al 0.01, Fe 0.1, Si 0.2.

† Resin 6877, Schenectady Chemicals Co.

Manuscript received April 22, 1985

Figure 2. Faceted grains grown in sintered boron carbide at 2250 °C. Notice cracks indicated by arrows. Etched specimen; bright field.

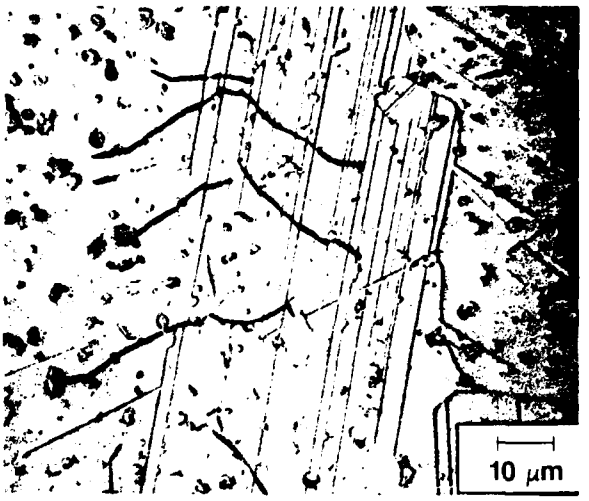

Figure 3. Transgranular microcracks in boron carbide. Notice also inclusions and engulfed grains. Etched specimen; bright field.

large faceted grains indicated the presence of a melt at temperature. However, the proximity to the eutectic temperature[8] and the presence of impurities detected by TEM as inclusions at some triple points, containing Si, Ti, Fe, and Cr, make the intervention of a liquid probable. The large grains invariably exhibit planar faults that were identified by electron diffraction in a thin section as twins with the twin direction $[01\bar{1}]$ or $[01\bar{1}\bar{1}]$. This is the expected orientation as it leaves the B_{12} icosahedra unsheared.[9] On the other hand, twinning in the small matrix grains was quite infrequent contrary to other observations.[10]

Sections of the coarsened microstructure with grains 100 μm and larger showed transgranular microcracks such as those in Figure 3. The crack density was low enough that the microcracking was not reflected in measurements of the elastic modulus or internal friction. In some instances, the cracks extended from the large grains into the fine-grain matrix indicating that the large grains were definitely the source of the stress that caused the cracking. The origin of the stresses could be attributed to thermal expansion anisotropy, however, no data to support it were found in the literature and, therefore, high temperature lattice parameter measurement was undertaken.

The B_4C used was identical with the powder identified above and was mixed with cubic BN as an internal standard,** one part of BN with 20 parts of B_4C by volume. The B_4C/BN mixture was applied in a slurry.

The lattice parameter measurements were carried out on a Rigaku high temperature diffractometer using Cu K-alpha radiation. Slit sizes were 2 × 0.45°. The measurements were carried out in a helium atmosphere, and data were collected at the following temperatures (°C) 24, 58, 102, 152, 201.5, 302, 402, 503.5, 604.5, 703, 801.5, 902.5, and 10.03. Six of the data collections were done over the two theta range 34-130° at counting times of 25-40 sec/0.05° increment; these were at temperatures 24, 152, 402, 703, 801.5, and 902.5°. The other collections were done over the two theta range 34-86° at counting times of 10 sec/0.05° increment.

The two theta values for B_4C at each temperature were corrected using the two known theta values for BN at that temperature. To assign indices to high angle reflections not given in the JCPDS file, the power pattern for B_4C was simulated using the Dean Smith program. The program B106A was used to calculate the lattice parameters.

At 700 °C and above, an amorphous phase began forming, and concurrently the lattice parameter measurements were not consistent with the measurements taken up to 600°; the lattice was smaller than was expected at 700 °C and above. The amorphous phase was probably B_2O_3. Because of this development, only data up to 600 °C were considered in the calculation of the thermal expansion coefficients for a and c.

The lattice parameters values, $\Delta a/a$, and $\Delta c/c$ at their respective temperatures, are given in Table 1 and are plotted in Figure 4. The slopes correspond $\Delta\alpha_a/\alpha_a = 5.29 \times 10^{-6}$ (0.29) and $\Delta\alpha_c/\alpha_c = 6.25 \times$

** The cubic boron nitride was provided by R.C. DeVries of the General Electric Research and Development Center.

Table 1

T (°C)	a_o Å	$a/a_o\ 10^{-4}$	c_o Å	$c/c_o\ 10^{-4}$
24	5.6039(12)	0	12.0756(25)	0.0
58	5.6030(22)	−1.606	12.0751(46)	−0.414
102	5.6038)17)	−0.178	12.0808(37)	4.306
152	5.6071(14)	5.710	12.0888(29)	10.931
201.5	5.6093(20)	9.636	12.0855(43)	8.198
302.0	5.6112(29)	13.027	12.0900(61)	11.925
402.0	5.6133(12)	16.774	12.1021(27)	21.945
503.5	5.6165(16)	22.484	12.1097(35)	28.239
604	5.6207(14)	29.979	12.1209(30)	37.514

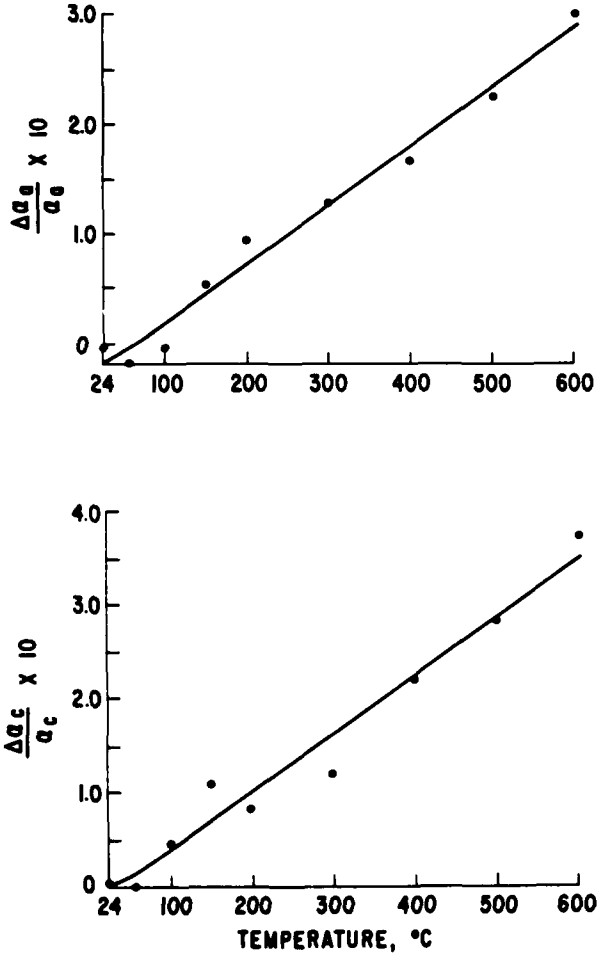

Figure 4. Lattice parameter values and their respective temperatures.

10^{-6} (0.44) where the data in parenthesis gives the standard errors. Averaging the data, i.e., $(2 \times \alpha_a + \alpha_c)/3$ gives $\bar{\alpha} = 5.61 \times 10^{-6}$ (0.34) in fair agreement with thermal expansion determined in a dilatometer on a sintered specimen of density 2.44 g/cc that gave $\bar{\alpha} = 5.25 \times 10^{-6}$.

The thermal expansion anisotropy is large enough to account for severe local stresses caused by the large temperature differential ($\Delta T \sim 2200$ °C) and modulus ($E = 4.4 \times 10^{11}$ Pa). Even in the case of the worst coincidence of errors, the residual stresses would reach 40 ksi. Such stresses may be responsible, at least in part, for the relatively low fracture strength currently observed in polycrystalline B_4C.

REFERENCES

1. P.S. Kislyi and B.L. Grabchuk, "Investigation of the Sintering of B_4C into Dense Bodies," *Proc. 4th Eur. Symp. on Powder Metal. 3,* 10-2 (1975).
2. B.L. Grabchuk and P.S. Kislyi "Some Features of the Sintering Behavior of Pure and Technical Boron Carbide," *Soviet Powder Met.* No. 9, 18-22 (1976).
3. J.W. Henney and J.W.S. Jones, Brit. Pat. #2014193, "Sintered Boron Carbide Containing Free Carbon," (1978).
4. H. Suzuki, T. Hasse, and T. Maruyama, "Effect of Carbon on Sintering or Boron Carbide," *Yogyo Kyokai Shi 87,* 430-433 (1979).
5. K. Schwetz and W. Grellner, "The Influence of Carbon on the Microstructure and Mechanical Properties of B_4C," *J. Less-Common Met. 82,* 37-47 (1981).
6. S. Prochazka and S.L. Dole, "Densification and Microstructure Development in Boron Carbide," *Proceedings of the 9th Annual Conference on Composites and Advanced Ceramics,* A. Cer. Soc. (1985).
7. Man F. Yan, "Microstructural Control in the Processing of Electronic Ceramics," *Mat. Sci. Eng. 48,* 53 (1981).

8. M. Beauvy, "Stoichiometric Limits of Boron Carbide Phases," *J. Less- Common Met. 90,* 169-175 (1983).
9. G. Will and K.H. Kossobutzki, "An X-ray Diffraction Analysis of Boron Carbide," *J. Less-Common Met. 44,* 87 (1976), *47,* 43 (1976).
10. A.K. Bandyopadhyay, F. Beunen, L. Zuppiroli, and M. Beauvy, "The Role of Free Carbon in the Transport and Magnetic Properties of Boron Carbide," *J. Phys. Chem. Solids 45,* 207-214 (1984).

END

FILMED

1-86

DTIC